2.6–2.7 Ga crustal growth in Yangtze craton, South China

Kang Chen [a], Shan Gao [a,b,*], Yuanbao Wu [a], Jingliang Guo [a], Zhaochu Hu [a], Yongsheng Liu [a], Keqing Zong [a], Zhengwei Liang [a], Xianlei Geng [a]

[a] State Key Laboratory of Geological Processes and Mineral Resources, Faculty of Earth Sciences, China University of Geosciences, Wuhan 430074, China
[b] State Key Laboratory of Continental Dynamics, Department of Geology, Northwest University, Xi'an 710069, China

ABSTRACT

A combined study of zircon U–Pb and Lu–Hf isotopes and whole rock major and trace elements and Sr–Nd isotopes has been conducted for 10 tonalitic–trondhjemitic–granodioritic (TTG) and granitic gneisses from the Kongling terrain, the only known Archean microcontinent in the Yangtze craton, South China. The results reveal a significant magmatic event at ~2.6–2.7 Ga, in addition to the previously reported ~2.9 Ga and ~3.2–3.3 Ga magmatism. The ~2.6–2.7 Ga rocks show relatively high REE (530–1074 ppm), apparently negative Eu anomaly (Eu/Eu* = 0.22–0.35), low #Mg (19.51–22.63) and low La_N/Yb_N (10.3–24.2). Besides, they have high K-feldspar proportion and relatively evaluated $(K_2O + Na_2O)/CaO$, TFeO/MgO, Zr, Nb, Ce and Y contents. Their $10,000 \times Ga/Al$ ratios range between 3.00 and 3.54. All these features suggest that the protoliths of these gneisses are A-type granites. Most of the ~2.6–2.7 Ga zircon grains have $\varepsilon_{Hf}(t)$ values >0 (up to 7.93, close to the depleted mantle value). This clearly indicates a considerably higher proportion of new crustal components in the ~2.6–2.7 Ga granitoids compared to the ~3.2–3.3 Ga and ~2.9 Ga TTGs. Our results support the conclusion of worldwide studies of igneous and detrital zircons that age peaks at 2.65–2.76 Ga represent increases in the volume of juvenile continental crust. The present study also confirms the existence of the two older magmatic events in the Kongling terrain. Both whole rock $\varepsilon_{Nd}(t)$ values (−3.74 to 1.59) and the zircon $\varepsilon_{Hf}(t)$ values (−11.18 to 3.55) for the ~2.9 Ga TTG and the Hf isotopes of ~3.2–3.3 Ga igneous zircons (−7.37 to 3.12) are chondritic or subchondritic, suggesting that they were mainly generated by reworking of older rocks with a small amount of new crustal additions.

© 2012 Elsevier B.V. All rights reserved.

1. Introduction

It is generally accepted that Archean terrains are volumetrically dominated by sodium-rich granitoids of tonalite–trondhjemite–granodiorite (TTG) suites (Condie, 1981; Jahn et al., 1981; Martin, 1987; Drummond and Defant, 1990). Consequently, the formation and tectonic significance of Archean TTGs are crucial for understanding the origin and evolution of early continental crust (e.g. Smithies et al., 2003; Condie, 2005; Martin et al., 2005; Moyen and Martin, 2012). Most Archean TTGs have experienced sophisticated subsequent reworking and alteration, which makes seeing back through time to the processes involved in their generation extraordinarily challenging. Nevertheless, it has been shown that the application of combined CL image, U–Pb and Lu–Hf isotope analyses of zircons can arguably provide more detailed and reliable information for Archean TTG suites than whole rock records (e.g. Vervoort and Blichert-Toft, 1999; Griffin et al., 2004; Davis et al., 2005; Halpin et al., 2005; Kemp et al., 2010; Zeh et al., 2011). Based on this robust cornerstone, many significant insights into the complex formation mechanisms of Archean cratons have been made over the past ten years, in particular into the issue whether such cratons sourced from accretion of new crustal additions or from the reworking of pre-existing crust (Andersen et al., 2002; Griffin et al., 2004; Woodhead et al., 2004; Gerdes and Zeh, 2009; Kemp et al., 2009; Hawkesworth et al., 2010; Zeh et al., 2010).

The North China and Yangtze cratons are the two largest Archean cratons in East China. They collided with each other along the E-W trending Qinling–Dabie–Sulu orogenic belt in the Triassic period (Rowley et al., 1997; Hacker et al., 1998; Ayers et al., 2002). The North China craton, which shows widespread Archean rocks dating back to ~3.8 Ga, has a complex and multi-stage growth history and has been well studied (Jahn et al., 1987; Liu et al., 1992, 2012a, b; Song et al., 1996; Zhao et al., 2001, 2005; Gao et al., 2004; Zheng et al., 2004; Kusky et al., 2007; Wu et al., 2008a; Zhai et al., 2010; Nutman et al., 2011; Peng et al., 2011, 2012b; Zhai and Santosh, 2011; Geng et al., 2012; Li et al., 2012; Lü et al., 2012). In

* Corresponding author at: State Key Laboratory of Geological Processes and Mineral Resources, Faculty of Earth Sciences, China University of Geosciences, Wuhan 430074, China. Tel.: +86 27 67884940; fax: +86 27 67885096.
E-mail address: sgao@263.net (S. Gao).

contrast, the Yangtze craton consists mainly of Proterozoic rocks with only sporadic outcrops of Archean basement in the Kongling terrain (Chen and Jahn, 1998; Gao et al., 1999, 2011; Qiu et al., 2000; Wu et al., 2012). A few studies have addressed the issues about TTG gneiss (Qiu et al., 2000; Zhang et al., 2006a; Jiao et al., 2009; Gao et al., 2011) and metasedimentary rocks (Gao et al., 1999, 2011; Qiu et al., 2000; Zhang et al., 2006b, 2006c; Liu et al., 2008a; Wu et al., 2009), which make up the principal part of the Kongling terrain. However, most of these studies are confined to the western part of the Kongling terrain. The eastern part is largely unknown.

In this work, we report whole rock major and trace elements and Sr–Nd isotopes, as well as zircon U–Pb ages and Hf isotopes for 10 TTG and granitic gneisses from the eastern part of the Kongling terrain (Fig. 1). Our results, for the first time, reveal a significant magmatic event at ~2.6–2.7 Ga, in addition to the previously reported ~2.9 Ga and ~3.2–3.3 Ga events. Therefore, the Kongling terrain experienced at least three Archean magmatic events.

2. Geological setting and samples

The South China block was formed by the Grenvillian-age continental collision (Li et al., 2002) between the Yangtze craton and the Cathaysia block. The Yangtze craton is bounded to the west by the Tibetan Plateau, to the north by the Qinling–Dabie–Sulu Orogen and to the south by the Jiangnan Orogen. Although some Archean zircons (xenocrystic) have been reported in different places in the Yangtze craton and in the northern Dabie Orogen (Zheng et al., 2006; Sun et al., 2008; Wu et al., 2008b), Archean outcrops within Yangtze craton have been only spotted in the Kongling terrain. The Kongling terrain, in an oval dome structure, covers an area of approximately 360 km^2 and is located at Xingshan and Zigui counties of Hubei province in the northwestern part of the Yangtze craton (Fig. 1). This Archean basement was intruded by the Quanqitang K-feldspar granite in a small scale at ~1.85 Ga (Xiong et al., 2009; Peng et al., 2012a) in the northern part and, in the southern part, by the bulky Huangling granitoid complex which comprises four suites: Huanglingmiao trondhjemite, Dalaoling granodiorite, Sandouping tonalite, and Xiaofeng tonalite (Fig. 1). Zircon U–Pb dating revealed that their ages are 800–820 Ma, 817 ± 22 Ma, 805 ± 9 Ma (Zhang et al., 2009) and 806 ± 4 Ma (Zhang et al., 2008), respectively. Owing to the bulky Huangling granitoid complex, the whole Kongling terrain was divided into northern and southern segments, referred to the North Kongling terrain and the South Kongling terrain (Gao et al., 2011). The Kongling terrain mainly consists of three types of rock associations (Gao and Zhang, 1990; Gao et al., 1999): (1) dioritic, tonalitic, trondhjemitic, granitic (DTTG) gneisses; (2) metasedimentary rocks; and (3) amphibolites and locally preserved mafic granulites, commonly occurring as lenses, boudins, and layers within gneisses (Fig. 1). The proportion of the felsic gneisses, clastic metasediments, and amphibolites is about 0.51, 0.44 and 0.05, respectively. It is worthy to note that approximately 90% DTTG and granitic gneisses in the Kongling terrain are exposed in the North Kongling terrain, as is displayed by geological mapping (Fig. 1).

Based on mineralogical, geochemical and Sr–Nd isotopic compositions, Gao et al. (1999) divided the clastic metasediments into three groups: (1) Group A shows no to slightly negative Eu anomalies, with Chemical Index of Alteration (CIW) close to felsic gneisses, high Cr and Ni contents and low Th and REE contents and is dominated by feldspar, biotite and quartz with variable garnet and amphibole; (2) Group B is characterized by negative Eu anomalies, high CIW and the presence of graphite and muscovite; (3) Group C is restite and contains abundant sillimanite, garnet and ilmenite. Qiu et al. (2000) provided the first evidence for the presence of >3.2 Ga sialic crust, using detrital zircons from two metapelites in the Kongling terrain. Detrital zircon U–Pb results

of eight Neoproterozoic sandstone and tillite samples from the south of the Kongling terrain reveal four major age populations of 720–910 Ma, 1.90–2.05 Ga, 2.40–2.55 Ga and 2.60–2.70 Ga with a few grains >3.2 Ga (Liu et al., 2008a). In addition, Zhang et al. (2006b) obtained an age of ~3.8 Ga for one detrital zircon from a Neoproterozoic sandstone.

Several attempts have been carried out to study the Kongling TTG gneisses in the light of igneous zircons, by employing SHRIMP and laser ablation inductively coupled plasma mass spectrometry (LA-ICP-MS). Qiu et al. (2000) first reported a magmatic event at ~2.90–2.95 Ga for two trondhjemitic gneisses (KY05 and KY17) in the western segment of the North Kongling terrain which was interpreted as the age of the trondhjemite emplacement (Fig. 1). In the same part of the Kongling terrain, similar results were also obtained by Zhang et al. (2006a) for two migmatites 04YC97 (2947 ± 28 Ma) and 04YC104 (2936 ± 28 Ma). Inherited zircon cores with ^{207}Pb/^{206}Pb ages of ~3.2 Ga were identified (Zhang et al., 2006a). Besides, Jiao et al. (2009) reported a protolith intrusion age of 3218 ± 13 Ma for a gneiss (06HL09) along the northeastern edge of the North Kongling terrain. Moreover, Gao et al. (2011) investigated two TTG gneisses (KH80 and KH84) along the southern margin of the North Kongling terrain. Zircon U-Pb results of sample KH84 suggested a magmatic event at 3302 ± 7/8 Ma. About 3.2–3.3 Ga inherited zircon cores were identified in KH80. Both samples were significantly affected by a ~2.8–2.9 Ga magmatism. These ages were, so far, the oldest known emplacement ages in the Kongling terrain. Available Hf isotope analyses of these gneisses reveal that the $\varepsilon_{Hf}(t)$ values vary between −11.18 and 3.00 and the corresponding two-stage depleted mantle Hf model ages (T_{DM2}) range from ~3.24 to ~3.81 Ga with a significant peak at 3.30–3.50 Ga (Zhang et al., 2006a; Jiao et al., 2009; Gao et al., 2011).

The present study investigated 10 TTG and granitic gneisses from the eastern part of the North Kongling terrain. The concrete localities and descriptions of all samples are shown in Fig. 1 and Table 1. It is merited to point out that some gray gneisses were cut by migmatitic K-feldspar-rich veins. However, all the studied rocks are free from the apparent migmatitic veins.

3. Analytical techniques

3.1. Whole rock element and Sr–Nd isotopic compositions

Major element compositions were measured by XRF (Rikagu RIX 2100) using fused glass disks at the State Key Laboratory of Continental Dynamics, Northwest University, China. Analyses of Chinese National basalt standard GBW07105 (GSR-3) and Chinese National syenite standard GBW07105 indicate that accuracy is better than 7% for all the oxides under investigation (Rudnick et al., 2004). Trace element analyses were conducted using an Agilent 7500a ICP-MS at the State Key Laboratory of Geological Processes and Mineral Resources, China University of Geosciences, Wuhan. The detailed sample-digestion procedure for ICP-MS analyses was reported in Liu et al. (2008b). Results obtained for USGS standards (AGV-2, BHVO-2, RGM-1 and BCR-2) show that analytical accuracies were better than 15% for most elements. Exceptions are Cr, Cu and Sn in BCR-2, which differ up to 19%, and Ni and Mo in RGM-1, which differ up to 25%.

Sr-Nd isotopic ratios were analyzed on a Triton TI mass spectrometer (Thermo Finnigan, Germany) operated in static mode at the State Key Laboratory of Geological Processes and Mineral Resources, China University of Geosciences, Wuhan. Full details of the Rb–Sr and Sm–Nd procedures were reported in Gao et al. (2004). ^{87}Rb/^{86}Sr and ^{147}Sm/^{144}Nd ratios were calculated from measured whole rock Rb, Sr, Sm and Nd contents determined by ICP-MS. The JNDi-1 and BCR-2 standards measured during
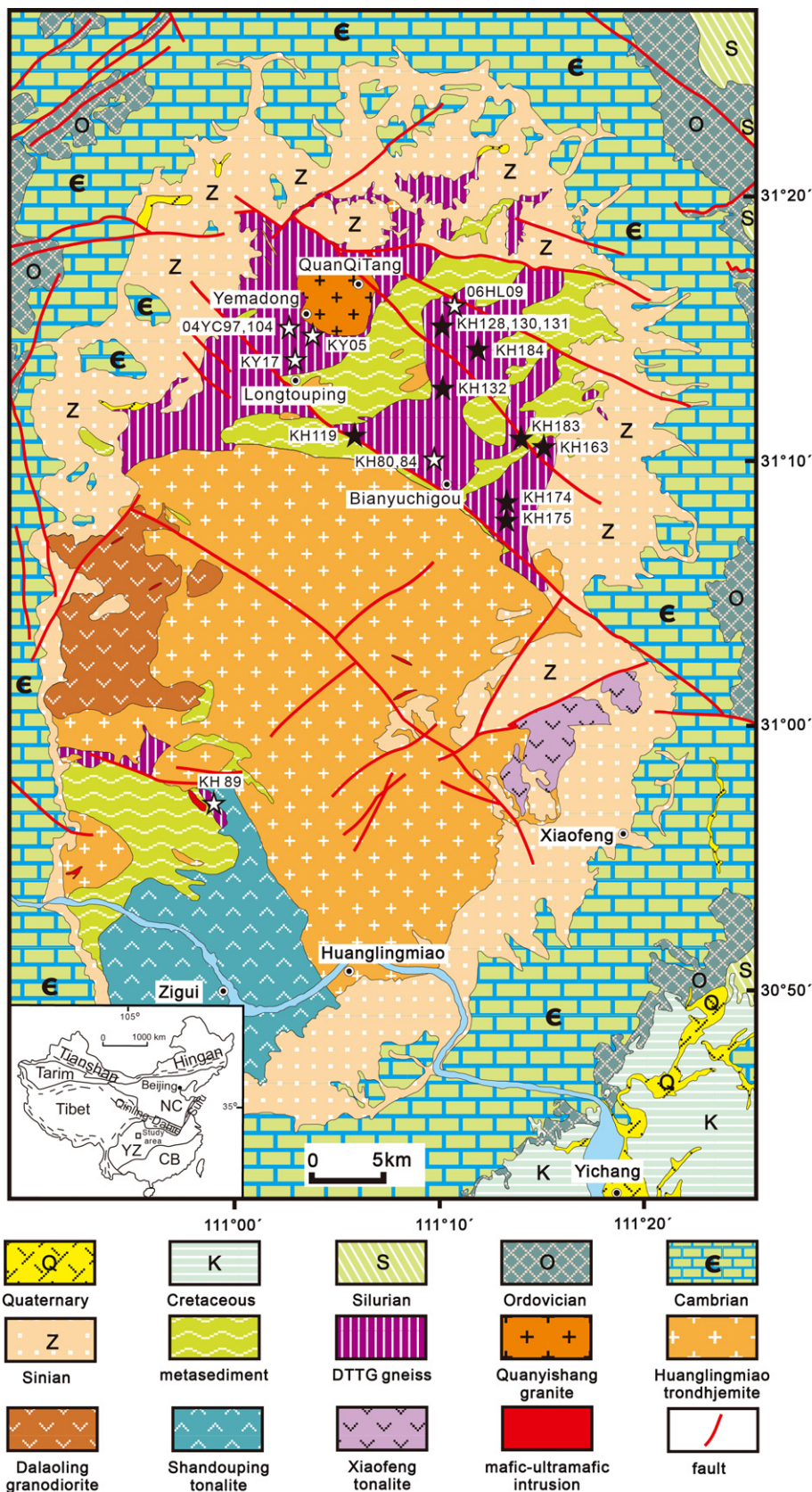
Fig. 1. Geological map of the Archean Kongling terrain. Inset shows major tectonic divisions of China, where YZ and SC denote the Yangtze craton and Cathaysia block, respectively (Modified after Gao et al., 2011). Open and filled stars indicate sample localities from previous studies and this investigation, respectively.

Table 1
Sample description and GPS co-ordinates.

Sample	Lithology	Latitude (°N)	Longitude (°E)	Mineral assemblage in the sample
KH119	Trondhjemitic gneiss	31°10′47.2″	111°05′46.1″	Pl(45%), Qtz(35%), Bi(10%)
KH128	A-type granitic gneiss	31°15′06.2″	111°10′04.6″	Kfs(50%), Qtz(25%), Pl(10%), Bi(5%)
KH130	A-type granitic gneiss	31°15′06.2″	111°10′04.6″	Kfs(45%), Qtz(30%), Pl(10%), Bi(5%)
KH131	A-type granitic gneiss	31°14′56.0″	111°10′12.7″	Kfs(50%), Qtz(25%), Pl(10%), Bi(5%)
KH132	Granitic gneiss	31°12′42.7″	111°10′11.5″	Pl(40%), Qtz(30%), Kfs(15%), Bi(5%)
KH163	Granitic gneiss	31°10′33.1″	111°15′05.4″	Pl(35%), Qtz(35%), Kfs(10%), Bi(10%)
KH174	A-type granitic gneiss	31°08′15.4″	111°13′18.3″	Kfs(60%), Qtz(20%), Pl(5%), Bi(5%)
KH175	Trondhjemitic gneiss	31°07′35.0″	111°12′56.3″	Pl(40%), Qtz(40%), Bi(10%)
KH183	Trondhjemitic gneiss	31°10′33.1″	111°14′0.03″	Pl(45%), Qtz(35%), Bi(10%)
KH184	Granitic gneiss	31°14′29.4″	111°11′40.7″	Pl(35%), Qtz(30%), Kfs(15%), Bi(10%)

Abbreviations. Bi, biotite; Kfs, K-feldspar; Ms, muscovite; Pl, plagioclase; Qtz, quartz.

the analytical course gave $^{143}Nd/^{144}Nd$ of 0.512094 ± 7 (2σ, $n = 1$) and 0.512611 ± 2 (2σ, $n = 1$), respectively. NISTSRM987 standard yielded $^{87}Sr/^{86}Sr = 0.710271 ± 8$ (2σ, $n = 2$).

3.2. Zircon CL imaging, U–Pb and Lu–Hf analyses

Zircons were separated by conventional magnetic and heavy-liquid methods and then were selected, according to size, color, shape and turbidity under a binocular microscope, and mounted on a double-sided tape, cast in epoxy resin and then polished to expose even and intermediate surfaces.

3.2.1. CL imaging

Prior to in situ U–Pb and Hf isotopic analyses, cathodoluminescence (CL) images of zircons were conducted by a Quanta 400 FEG High Resolution Emission Field Environmental Scanning Electron Microscope connected to an Oxford INCA350 energy dispersive system (EDS) and a Gatan Mono CL3+ cathodoluminescence (CL) system at the State Key Laboratory of Continental Dynamics, Northwest University.

3.2.2. LA-ICP-MS U–Pb dating

U–Pb dating and trace element analyses of zircon were conducted synchronously by LA-ICP-MS at the State Key Laboratory of Geological Processes and Mineral Resources, China University of Geosciences, Wuhan. Laser sampling was performed using a GeoLas 2005 excimer ArF laser-ablation system (Lambda Physik, Göttingen, Germany). An Agilent 7500a ICP-MS instrument was used to acquire ion-signal intensities. Detailed operating conditions for the laser ablation system and the ICP-MS instrument and data processing are the same as description by Liu et al. (2008c, 2010a, b).

Our measurements of the reference zircon GJ-1 treated as an unknown during the runs of the Kongling zircons yielded a weighted mean $^{206}Pb/^{238}U$ age of 599.8 Ma (1σ, MSWD = 6, $n = 40$), which is in good agreement with the apparent ID-TIMS $^{206}Pb/^{238}U$ ages of 598.3–602.7 Ma (Jackson et al., 2004).

3.2.3. LA-MC-ICP-MS Lu–Hf analyses

Hf isotope analysis was carried out on a Neptune Plus MC-ICP-MS (Thermo Fisher Scientific, Germany), in combination with the GeoLas 2005 in the State Key Laboratory of Geological Processes and Mineral Resources, China University of Geosciences, Wuhan. Detailed operating conditions for the laser ablation system and the MC-ICP-MS instrument and data calibrating and processing were reported in Hu et al. (2012). The major limitation to accurate in situ zircon Hf isotope determination by LA-MC-ICP-MS is the very large isobaric interference from ^{176}Yb and, to a much lesser extent ^{176}Lu on ^{176}Hf (Woodhead et al., 2004). Interference of ^{176}Lu on ^{176}Hf was corrected by measuring the intensity of the interference-free ^{175}Lu isotope and using the recommended $^{176}Lu/^{175}Lu$ ratio of 0.02656 (Blichert-Toft et al., 1997) to calculate $^{176}Lu/^{177}Hf$ ratios. Similarly,

the interference of ^{176}Yb on ^{176}Hf was corrected by measuring the interference-free ^{173}Yb isotope and using the recommended $^{176}Yb/^{173}Yb$ ratio of 0.7962 (Chu et al., 2002) to calculate $^{176}Hf/^{177}Hf$ ratios. The analysis was done on the similar age domains of age determinations, as guided by CL images. Off-line selection and integration of analytical signals, and mass bias calibrations were performed using ICPMSDataCal (Liu et al., 2010a).

The obtained $^{176}Hf/^{177}Hf$ ratios using this technique are 0.2822905 ± 0.0000035 (1σ, MSWD = 2.6, $n = 89$) for 91500, 0.282019 ± 0.000004 (1σ, MSWD = 4.5, $n = 87$) for GJ-1. These results are identical, within 2σ, with the recommended $^{176}Hf/^{177}Hf$ ratios for 91500 (0.2823075 ± 58, 2σ) (Griffin et al., 2006; Wu et al., 2006) and GJ-1 (0.282015 ± 0.000019, 2σ) (Elhlou et al., 2006).

3.2.4. Constants and calculation parameter

A decay constant of $1.865 × 10^{-11}$ a^{-1} for ^{176}Lu (Scherer et al., 2001; Soderlund et al., 2004), present-day $^{176}Hf/^{177}Hf = 0.282772$ and $^{176}Lu/^{177}Hf = 0.0332$ for the chondritic uniform reservoir (CHUR) (Blichert-Toft and Albarede, 1997), present-day $^{176}Hf/^{177}Hf = 0.28325$ and $^{176}Lu/^{177}Hf = 0.0384$ for the depleted mantle (Griffin et al., 2000) and a mean value of $^{176}Lu/^{177}Hf = 0.0093$ for the upper continental crust (Vervoort and Patchett, 1996) were employed in this study. The initial $^{176}Hf/^{177}Hf$ ($^{176}Hf/^{177}Hf(t)$) ratio of respective zircon domain was calculated using the measured $^{207}Pb/^{206}Pb$ ages, $^{176}Hf/^{177}Hf$ values and $^{176}Lu/^{177}Hf$ values of each spot (Appendix Table 2). The single-stage model ages (T_{DM1}) of respective zircon domains were calculated relative to the depleted mantle recommended in Griffin et al. (2000).

Supplementary data related to this article found, in the online version, at http://dx.doi.org/10.1016/j.precamres.2012.10.017.

For the calculation of initial ε_{Hf} values ($\varepsilon_{Hf}(t)$) and the two-stage model ages (T_{DM2}), two steps were taken. First, the $^{176}Hf/^{177}Hf(t)$ value of respective zircon domain was calculated using the measured $^{207}Pb/^{206}Pb$ age, $^{176}Hf/^{177}Hf$ value and $^{176}Lu/^{177}Hf$ value of each spot. By means of this procedure, many zircon analyses from individual gneiss samples plot on linear arrays or have, within error, similar $^{176}Hf/^{177}Hf(t)$ ratios in the $^{176}Hf/^{177}Hf(t)$ vs $^{207}Pb/^{206}Pb$ age diagrams (Fig. 7). Given the case that the initial $^{176}Hf/^{177}Hf$ values of all of these zircon analyses are identical, within error, such an array or similarity suggests that all these zircons crystallized at the same time, but some of them underwent multiple Pb loss subsequently, while maintaining similar $^{176}Hf/^{177}Hf(t)$ ratios (Amelin et al., 2000; Zeh et al., 2007; Gerdes and Zeh, 2009). Second, for cores older than 3.0 Ga, the values of $\varepsilon_{Hf}(t)$ and T_{DM2} were calculated using the weighted average age of the concordant cores. Similarly, for rims younger than 2.1 Ga, the values of $\varepsilon_{Hf}(t)$ and T_{DM2} were calculated using the weighted average age of the concordant rims. For other zircon analyses that plot on such an array or have similar $^{176}Hf/^{177}Hf(t)$ ratios, the values of $\varepsilon_{Hf}(t)$ and T_{DM2} were calculated employing the respective magma crystallization age of each
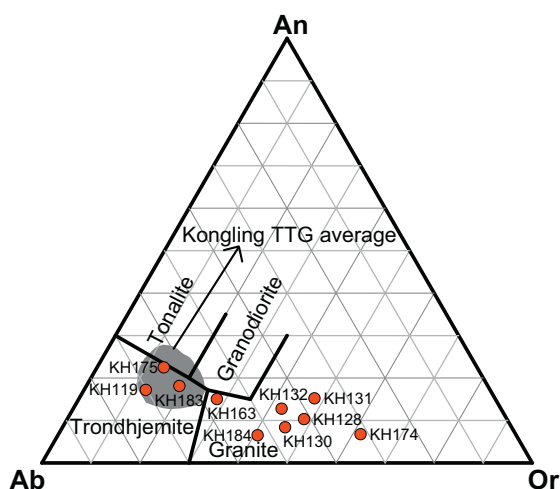
Fig. 2. Classification of the TTG and granitic rocks from the Kongling terrain using normative anorthite (An), albite (Ab) and orthoclase (Or), with fields defined by Barker (1979).

sample, determined by the weighted average age of concordant (98–102% concordance level) analyses (Appendix Table 2).

4. Analytical results

4.1. Major and trace element compositions

Results of major and trace elemental analyses of the 10 gneisses from the Kongling terrain are listed in Table 2. All the investigated samples display high SiO_2 (67–76 wt%) contents with elevated Na_2O contents (3.13–5.68 wt%) except KH131 (2.56 wt%) and KH174 (1.96 wt%). Their K_2O contents range from 1.30 to 5.46 wt% and Al_2O_3 from 11.11 to 16.00 wt%. They are poor in ferromagnesian ($TFe_2O_3 + MgO + MnO + TiO_2 = 2.22$–6.06 wt%). Based on the normative An–Ab–Or triangle classification for granitoid containing more than 10% modal or normative quartz (O'Connor, 1965; Barker, 1979), seven samples (KH128, KH130, KH131, KH132, KH163, KH174 and KH184) plot in the granite field and the other three samples (KH119, KH175 and KH183) plot in the trondhjemite field (Fig. 2).

According to REE distribution and trace element spider plots (Fig. 3a and b), two obvious groups can be divided. Group I (blue symbols in Fig. 3a and b) have relatively high REE (530–1074 ppm), apparently negative Eu anomaly (Eu/Eu* = 0.22–0.35), low #Mg (19.51–22.63) (molar $100 \times Mg/(Mg + Fe)$) and low La_N/Yb_N (10.3–24.2). They are intensively depleted in Sr–Eu–Ti and weakly depleted in Nb and Ta, typical features of A-type granites (Whalen et al., 1987; Eby, 1990; Bonin, 2007). In contrast, Group II (red and green symbols in Fig. 3a and b) exhibits lower REE (71.4–166 ppm), slightly or no negative Eu anomaly (0.56–1.09), higher #Mg (34.1–59.42) and elevated La_N/Yb_N (10.4–87.3). They are enriched in Pb and depleted in Nb–Ta–Ti, typical features of TTG suites (Jahn et al., 1981; Martin, 1994; Condie, 2005; Martin et al., 2005; Moyen and Martin, 2012). The characteristics of mineralogy and geochemistry of these rocks suggest that samples KH128, KH130, KH131 and KH174 are A-type granitic gneisses, KH132, KH163 and KH184 are granitic gneisses and KH119, KH175 and KH183 are TTG gneisses.

4.2. Zircon CL images, U–Pb and Lu–Hf analyses

4.2.1. A-type granitic gneisses
4.2.1.1. KH128.
For this sample, 33 in situ U–Pb dating analyses were carried out (Appendix Table 1). CL images of most zircon
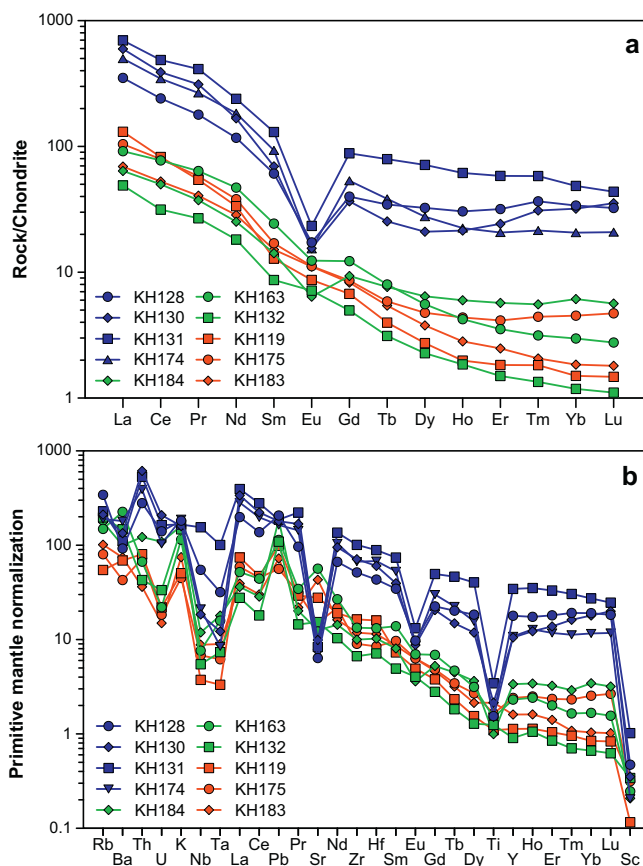

Fig. 3. Chondrite-normalized rare earth element patterns (a) and primitive mantle-normalized trace element distributions (b) of rocks from the Kongling terrain. Blue, green and red symbols denote A-type granitic, granitic and trondhjemitic gneisses, respectively. Chondrite and primitive mantle values are taken from Taylor and McLennan (1985) and McDonough and Sun (1995), respectively. (For interpretation of the references to color in this figure legend, the reader is referred to the web version of this article.)

crystals display oscillatory zoning with dark and thin overgrowth and some grains are structureless or complex (Fig. 4a). All the Th/U ratios of the zircons from this sample are >0.3 (0.31–0.62) (Fig. 5). The individual $^{207}Pb/^{206}Pb$ ages range from 2450 to 2733 Ma and 19 concordant analyses yield relatively similar $^{207}Pb/^{206}Pb$ ages (2591–2698 Ma), with a weighted average of 2645 ± 15 Ma ($n = 19$, MSWD = 0.9) (Fig. 6a). This age is identical, within error, to the upper intercept age of 2625 ± 23 Ma ($n = 33$, MSWD = 2.1) formed by 14 discordant analyses plus the 19 concordant analyses (Fig. 6a). Hence, the time of 2645 ± 15 Ma is interpreted as the intrusion age of this sample.

Supplementary data related to this article found, in the online version, at http://dx.doi.org/10.1016/j.precamres.2012.10.017.

A total of 29 Lu–Hf analyses were obtained (Appendix Table 2). As shown in Fig. 7a, all Lu–Hf analyses have homogeneous initial $^{176}Hf/^{177}Hf$ ratios of 0.281109–0.281196. Their $\varepsilon_{Hf}(t)$ values range between 0.52 and 3.60 and T_{DM2} values between 2842 and 3027 Ma (Appendix Table 2).

4.2.1.2. KH130.
A total of 28 zircon spots for KH130 were analyzed for U–Pb isotopes (Appendix Table 1). Most zircon domains are weakly zoned and some display a complex structure (Fig. 4b). All the Th/U ratios of the 28 spots are >0.3 (Fig. 5). Like KH128, it yields $^{207}Pb/^{206}Pb$ ages of 2435–2658 Ma and a weighted average of 2622 ± 14 Ma ($n = 15$, MSWD = 0.4) is produced by 15 concordant age spots (Fig. 6b). This age is identical with the upper intercept age of 2622 ± 19 Ma ($n = 28$, MSWD = 2.9) (Fig. 6b). Thus, the concordia

Table 2
Chemical compositions of rocks from Kongling terrain, South China.

	KH119	KH128	KH130	KH131	KH132	KH163	KH174	KH175	KH183	KH184
SiO_2	71.4	71.5	72.4	70.7	71.3	70.7	76.4	72.3	67.9	72.3
TiO_2	0.22	0.31	0.43	0.69	0.25	0.30	0.30	0.33	0.43	0.20
Al_2O_3	15.3	13.8	13.2	12.7	13.7	15.7	11.1	13.7	16.0	14.6
TFe_2O_3	2.28	2.97	3.41	5.21	2.50	1.78	2.53	3.20	3.34	1.48
TFeO	2.05	2.67	3.07	4.69	2.25	1.60	2.28	2.88	3.01	1.33
MnO	0.02	0.06	0.06	0.06	0.03	0.02	0.02	0.04	0.03	0.02
MgO	0.59	0.36	0.47	0.62	1.83	0.66	0.37	1.05	1.44	0.67
CaO	2.47	1.48	1.09	2.02	1.53	2.12	0.70	2.65	2.59	0.93
Na_2O	5.68	3.15	3.28	2.56	3.13	4.66	1.96	4.27	5.00	4.18
K_2O	1.46	5.26	4.62	4.79	4.26	3.31	5.46	1.30	2.16	4.62
P_2O_5	0.10	0.13	0.09	0.12	0.05	0.11	0.03	0.09	0.15	0.07
LOI	0.60	0.96	0.79	0.57	0.97	0.81	0.71	0.68	0.75	0.82
TOTAL	100	100	99.8	100	99.5	100	99.6	99.6	99.8	99.9
#Mg	34.10	19.51	21.61	19.22	59.42	42.58	22.63	39.62	46.30	47.52
TFeO/MgO	3.48	7.42	6.53	7.56	1.23	2.43	6.15	2.74	2.09	1.99
$(Na_2O + K2O)/CaO$	2.89	5.68	7.25	3.64	4.83	3.76	10.60	2.10	2.76	9.46
Li	14.2	10.9	7.77	9.85	13.4	26.3	4.32	11.0	25.3	10.3
Be	1.37	6.52	1.40	2.31	0.82	2.42	1.00	1.54	1.39	1.67
Sc	1.87	7.64	5.69	16.5	5.53	3.99	3.33	5.10	5.39	3.37
V	28.7	6.00	6.71	8.73	32.8	19.4	4.41	25.7	39.0	13.4
Cr	15.4	8.82	6.71	21.6	106	4.95	1.88	4.94	7.74	5.29
Co	5.28	3.31	4.90	4.90	11.6	4.21	2.29	8.54	7.24	3.15
Ni	6.51	6.16	5.47	9.35	75.3	3.79	2.56	8.64	6.19	3.49
Cu	4.11	9.97	45.3	2.52	23.4	7.12	24.2	21.7	3.32	13.4
Zn	30.3	47.9	36.6	77.7	48.0	46.5	30.1	40.7	66.6	27.5
Ga	17.7	24.1	21.0	23.8	15.9	20.1	18.6	17.1	21.1	19.6
Rb	32.8	205	127	137	118	89.3	114	48.1	60.8	105
Sr	552	127	197	166	305	1123	141	302	855	249
Y	4.85	76.9	45.2	148	3.89	9.93	46.5	10.3	6.90	14.5
Zr	172	540	746	1058	69.9	140	702	94.6	124	105
Nb	2.46	36.0	12.13	102	3.60	5.02	13.9	4.47	5.79	7.83
Mo	0.38	3.56	3.05	5.76	1.00	0.15	0.74	0.19	0.13	0.12
Sn	0.49	3.86	0.35	3.53	0.47	2.52	2.95	1.01	1.73	1.73
Cs	0.94	1.77	1.31	1.52	2.32	1.86	0.68	1.79	2.14	1.36
Ba	454	609	884	735	974	1488	1188	282	490	659
La	48.0	129	219	255	17.9	33.6	183	38.2	25.4	23.4
Ce	78.9	230	372	466	30.1	74.0	331	75.9	50.4	47.8
Pr	7.44	24.5	42.6	56.4	3.67	8.74	36.5	7.94	5.56	5.12
Nd	23.8	83.3	119	170	12.9	33.4	131	27.0	20.3	17.9
Sm	2.96	14.0	16.0	30.1	2.00	5.63	21.5	3.92	3.49	3.27
Eu	0.76	1.5	1.3	2	0.62	1.08	1.3	1.0	0.96	0.6
Gd	2.06	12.2	11.18	26.9	1.52	3.75	16.3	2.63	2.53	2.86
Tb	0.23	2.00	1.47	4.60	0.18	0.46	2.22	0.34	0.31	0.44
Dy	1.04	12.4	7.99	27.1	0.87	2.12	10.5	1.81	1.44	2.45
Ho	0.17	2.59	1.82	5.24	0.16	0.36	1.91	0.37	0.24	0.51
Er	0.46	7.91	6.04	14.51	0.37	0.88	5.15	1.03	0.62	1.42
Tm	0.06	1.30	1.10	2.07	0.05	0.11	0.76	0.16	0.07	0.20
Yb	0.37	8.40	7.93	12.03	0.29	0.74	5.12	1.12	0.46	1.52
Lu	0.06	1.23	1.35	1.66	0.04	0.11	0.79	0.18	0.07	0.21
Hf	4.51	12.2	17.1	25.1	2.02	3.73	19.2	2.39	3.24	2.90
Ta	0.12	1.18	0.45	3.72	0.27	0.59	0.31	0.23	0.33	0.66
Tl	0.24	0.88	0.67	0.66	0.68	0.69	0.63	0.41	0.50	0.80
Pb	14.8	30.9	26.9	28.0	16.3	17.1	24.6	8.41	10.9	27.9
Th	6.38	22.2	48.7	42.3	3.40	5.32	31.0	5.70	2.88	9.70
U	0.44	2.85	4.22	3.32	0.68	0.45	2.10	0.37	0.30	2.21
REE	166	530	809	1074	70.8	165	746	162	112	108
La_N/Yb_N	87.3	10.3	18.6	14.3	41.4	30.8	24.2	23.1	37.5	10.4
10000 Ga/Al	2.19	3.29	3.00	3.54	2.20	2.42	3.16	2.35	2.49	2.54
Eu/Eu*	0.93	0.35	0.31	0.22	1.09	0.72	0.22	0.93	0.99	0.56

Major element concentrations are reported in weight percent and trace and rare element concentrations in parts per million (ppm).

age of 2622 ± 14 Ma is interpreted as the emplacement time of this sample.

Twenty-five zircon spots were analyzed for Lu–Hf isotopes (Appendix Table 2). The results reveal that 23 spots have relatively homogeneous initial $^{176}Hf/^{177}Hf$ ratios between 0.281102 and 0.281179 with the other two analyses of 0.281065 and 0.281249 (Fig. 7b). Their $\varepsilon_{Hf}(t)$ values range from -1.57 to 5.04 and T_{DM2} values from 2745 to 3094 Ma (Appendix Table 2).

4.2.1.3. KH131. Thirty-three dating spots were conducted for this sample (Appendix Table 1). The CL images reveal that some zircon

grains have oscillatory zoning and others are completely structureless (Fig. 4c). Furthermore, the Th/U ratios of these 33 zircons are 0.16–0.52 with an average of 0.38 (Fig. 5). Their $^{207}Pb/^{206}Pb$ ages range from 2273 to 2694 Ma (Appendix Table 1) and 14 concordant analyses yield a weighted average of 2640 ± 18 Ma ($n = 14$, MSWD = 0.7). This age is slightly older than the upper intercept age of 2600 ± 18 Ma ($n = 33$, MSWD = 1.2) (Fig. 6c). The concordant age of 2640 ± 18 Ma is interpreted as the intrusion age of this sample.

Relatively homogeneous initial $^{176}Hf/^{177}Hf$ ratios of 0.281069–0.281220 were obtained from 28 Lu–Hf analyses (Appendix Table 2). However, another analysis (KH131-02) yields
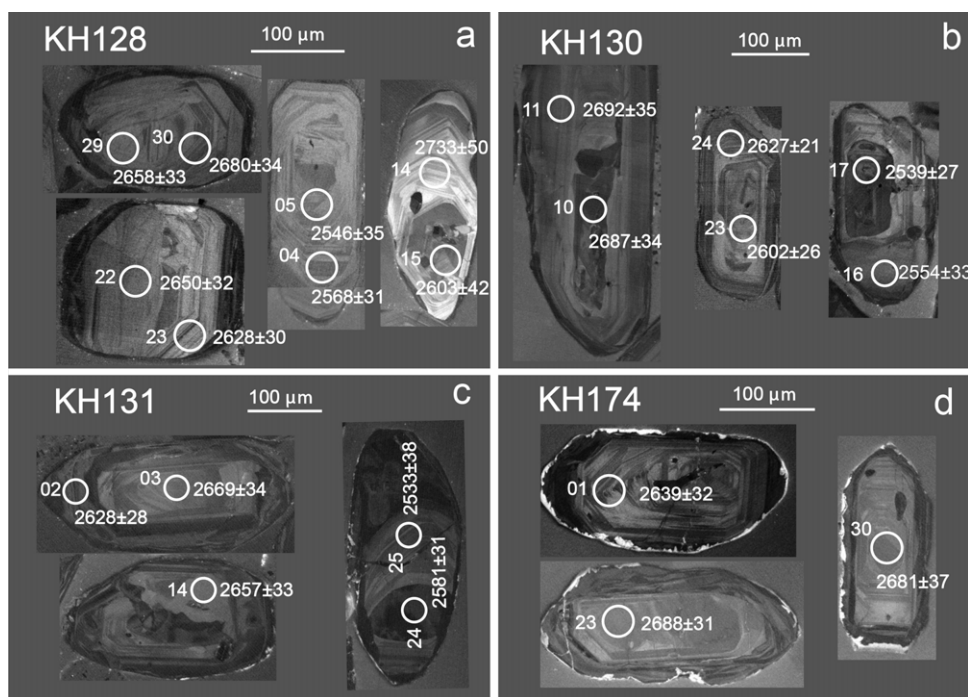
Fig. 4. Typical cathodoluminescence images of zircons for samples KH128 (a), KH130 (b), KH132 (c) and KH174 (d) from the Kongling terrain. White circles (32 μm) indicate position of laser spots. Numbers on the left and right sides of each spot indicate analytical number and the Pb–Pb age with 1σ error (in Ma).

a higher initial ratio of 0.281292 (Fig. 7c). All the $\varepsilon_{Hf}(t)$ values range between −0.98 and 6.96 and their T_{DM2} values vary from 2679 to 3079 Ma (Appendix Table 2).

4.2.1.4. KH174. For this sample, twenty-four U–Pb analyses were acquired (Appendix Table 1). Most of these zircons are weakly zoned and some of them display a core–rim structure (Fig. 4d) in which the rims are structureless and thin. The Th/U ratios of almost all analyses are >0.3 (Fig. 5). The ^{207}Pb/^{206}Pb ages of 17 concordant analyses range from 2613 to 2728 Ma with a weighted average age of 2671 ± 17 Ma ($n = 17$, MSWD = 0.8) (Fig. 6d). This age, within error, agrees well with the upper intercept age of 2685 ± 19 Ma ($n = 24$, MSWD = 0.6) obtained from all spots (Fig. 6d). The concordant age of 2671 ± 17 Ma is interpreted as the time of the protolith intrusion.
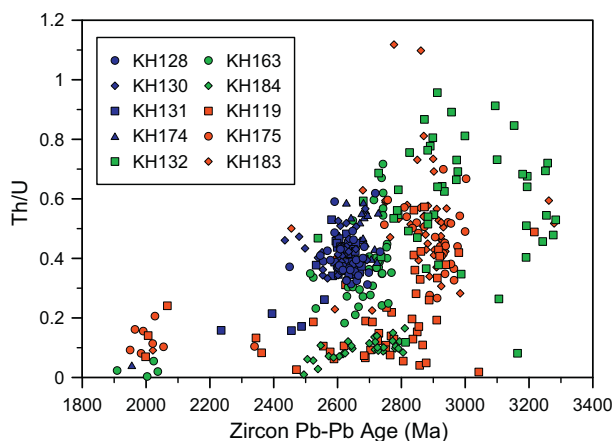
Fig. 5. Variation of zircon Th/U ratio with age for sample from the Kongling terrain. Blue, green and red symbols denote A-type granitic, granitic and trondhjemitic gneisses, respectively. (For interpretation of the references to color in this figure legend, the reader is referred to the web version of this article.)

Lu–Hf analyses were conducted on 18 zircon spots (Appendix Table 2). The results reveal that they show a larger scatter of initial ^{176}Hf/^{177}Hf ratios between 0.280804 and 0.281299 (Fig. 7d). However, 14 Hf isotopic analyses yield relatively homogeneous initial ^{176}Hf/^{177}Hf ratios of 0.281148–0.281299 (Fig. 7d). Their $\varepsilon_{Hf}(t)$ values vary from 2.54 to 7.93 and their T_{DM2} values are between 2650 Ma and 2927 Ma (Appendix Table 2). The other four analyses have considerably lower initial ^{176}Hf/^{177}Hf ratios below 0.2810. Their CL images and Th/U ratios are similar to those yielding higher initial ^{176}Hf/^{177}Hf ratios and they are all nearly concordant (97–100% concordance level). Their $\varepsilon_{Hf}(t)$ values range between −9.67 to −2.71 and their T_{DM2} values are of 3186–3514 Ma (Appendix Table 2).

4.2.2. Granitic gneisses
4.2.2.1. KH184. Thirty U–Pb dating spots were conducted for this sample (Appendix Table 1). Compared to those zircons discussed in the foregoing samples, zircons from KH184 are much smaller and darker (Fig. 8a). Some of them exhibit weakly oscillatory zoning patterns and some are structureless (Fig. 8a). Their Th/U ratios are of 0.01–0.17 (Fig. 5). Nine concordant analyses have ^{207}Pb/^{206}Pb ages between 2633 and 2727 Ma with a weighted average of 2691 ± 32 Ma ($n = 9$, MSWD = 1.6). This age is similar to or slightly younger than the upper intercept age of 2729 ± 20 Ma ($n = 24$, MSWD = 1.2) formed by the nine concordant analyses plus 15 discordant analyses (Fig. 9a). The concordant age of 2691 ± 32 Ma is interpreted as the crystallization age of this sample.

Relatively homogeneous initial ^{176}Hf/^{177}Hf ratios between 0.280992 and 0.281123 were obtained from 18 Lu–Hf analyses (Appendix Table 2 and Fig. 7e). All the $\varepsilon_{Hf}(t)$ values are of −2.48 to 2.08 and their T_{DM2} values vary from 2965 Ma to 3174 Ma (Appendix Table 2).

4.2.2.2. KH163. CL images of most zircon domains reveal a core–rim structure (Fig. 8b). As shown in Fig. 9b, 45 U–Pb age analyses reveal two age populations from the rims and the cores (Appendix Table 1):
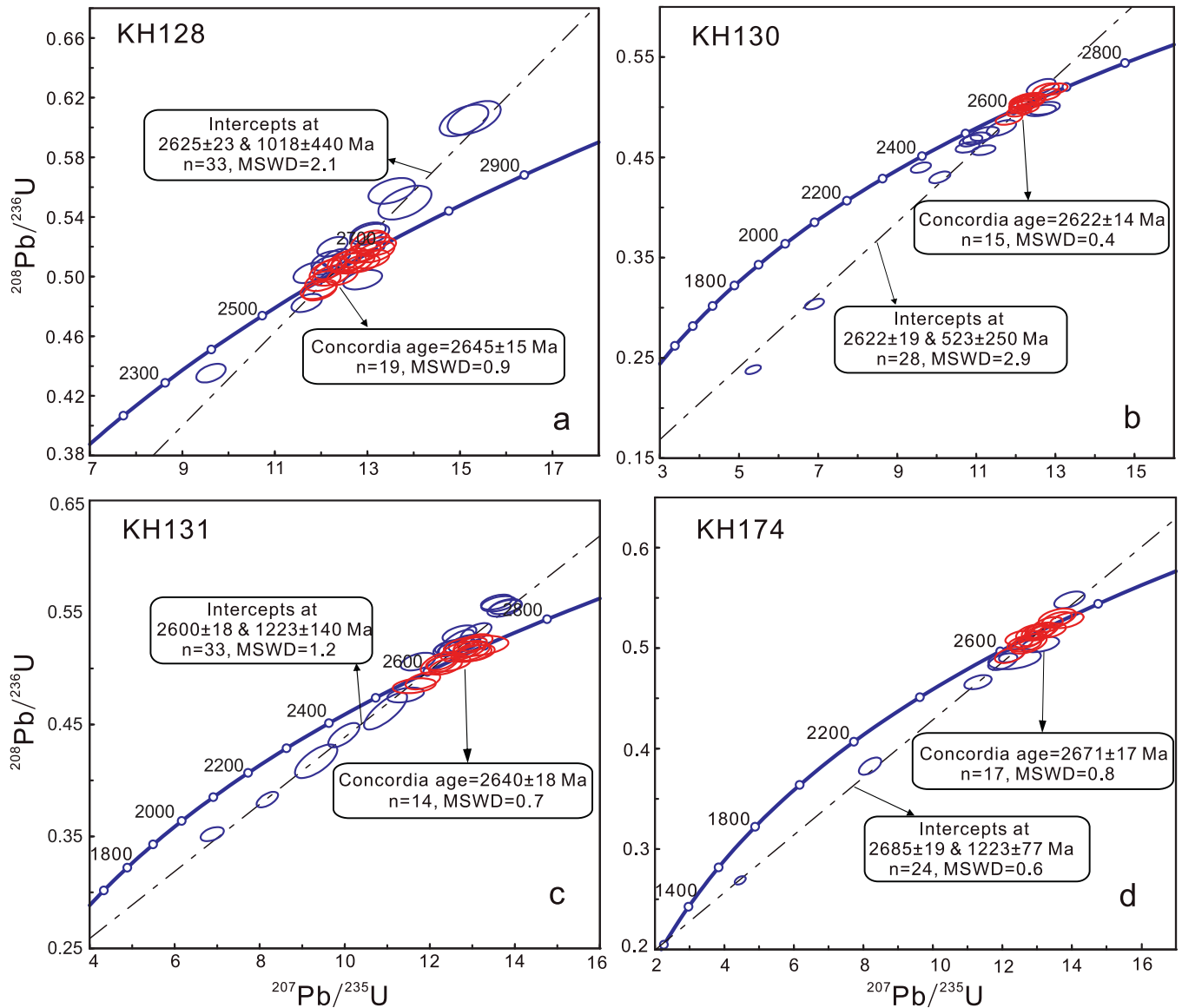
Fig. 6. Zircon U–Pb concordia plots for samples KH128 (a), KH130 (b), KH132 (c) and KH174 (d) from the Kongling terrain. Red and blue ellipses indicate concordant and discordant analyses, respectively. Errors are $\pm 1\sigma$. (For interpretation of the references to color in this figure legend, the reader is referred to the web version of this article.)

(1) 2.6–2.7 Ga, which is represented by 15 concordant U–Pb analyses with apparent $^{207}Pb/^{206}Pb$ ages between 2622 Ma and 2759 Ma (Appendix Table 1). CL images of these zircon crystals reveal two dark zones (cores and rims), which are separated by a bright and thin band (Fig. 8b). Most of the cores are characterized by oscillatory zoning patterns but rims are weakly zoned or structureless (Fig. 8b). They have Th/U ratios ranging from 0.18 to 0.62 with an average of 0.38 (Fig. 5). They give a weighted average $^{207}Pb/^{206}Pb$ age of 2707 ± 24 Ma ($n = 15$, MSWD = 1.9), which is, within error, consistent with the upper intercept age of 2681 ± 37 Ma ($n = 40$, MSWD = 2.3) produced by four rim and 15 concordant and 21 discordant core analyses (Fig. 9b). The concordant age is interpreted as the emplacement age of the trondhjemitic magma.

(2) ~2.0 Ga, which is denoted by three concordant rim spots with $^{207}Pb/^{206}Pb$ ages of 2003 ± 33 Ma, 2024 ± 35 Ma and 2037 ± 38 Ma (Fig. 9b). CL images reveal that they occur as rims with weakly oscillatory zoning (Fig. 8b) and their Th/U ratios are 0.01–0.05 (Fig. 5). This age is interpreted as the time of a subsequent metamorphic event.

Thirty-nine age spots were conducted for Lu–Hf analyses (Appendix Table 2), of which 37 core spots yield relatively homogeneous initial $^{176}Hf/^{177}Hf$ ratios of 0.280972–0.281089 (Fig. 7f). Their $\varepsilon_{Hf}(t)$ and T_{DM2} are between −3.19 and 0.95 and between 3006 Ma and 3204 Ma, respectively (Appendix Table 2). The other two Lu–Hf analyses were carried out on the rims (KH163-36 and KH163-55), yielding relatively higher initial $^{176}Hf/^{177}Hf$ ratios of 0.281095 and 0.281107 (Fig. 7f). Their $\varepsilon_{Hf}(t)$ values are −14.39 and −13.92 and their T_{DM2} values are 3251 and 3194 Ma, respectively (Appendix Table 2).

4.2.2.3. KH132. For this sample, 47 U–Pb dating spots were carried out (Appendix Table 1). Almost all zircon grains display a core–rim structure (Fig. 8c). The rims are too thin to be dated so the ages were all obtained from zircon cores. As shown in Fig. 9c, two age populations can be divided:

(1) 3.1–3.2 Ga, which is represented by 7 concordant analyses with apparent $^{207}Pb/^{206}Pb$ ages of 3164–3284 Ma (Appendix Table 1). As displayed in CL images (Fig. 8c), most of these age
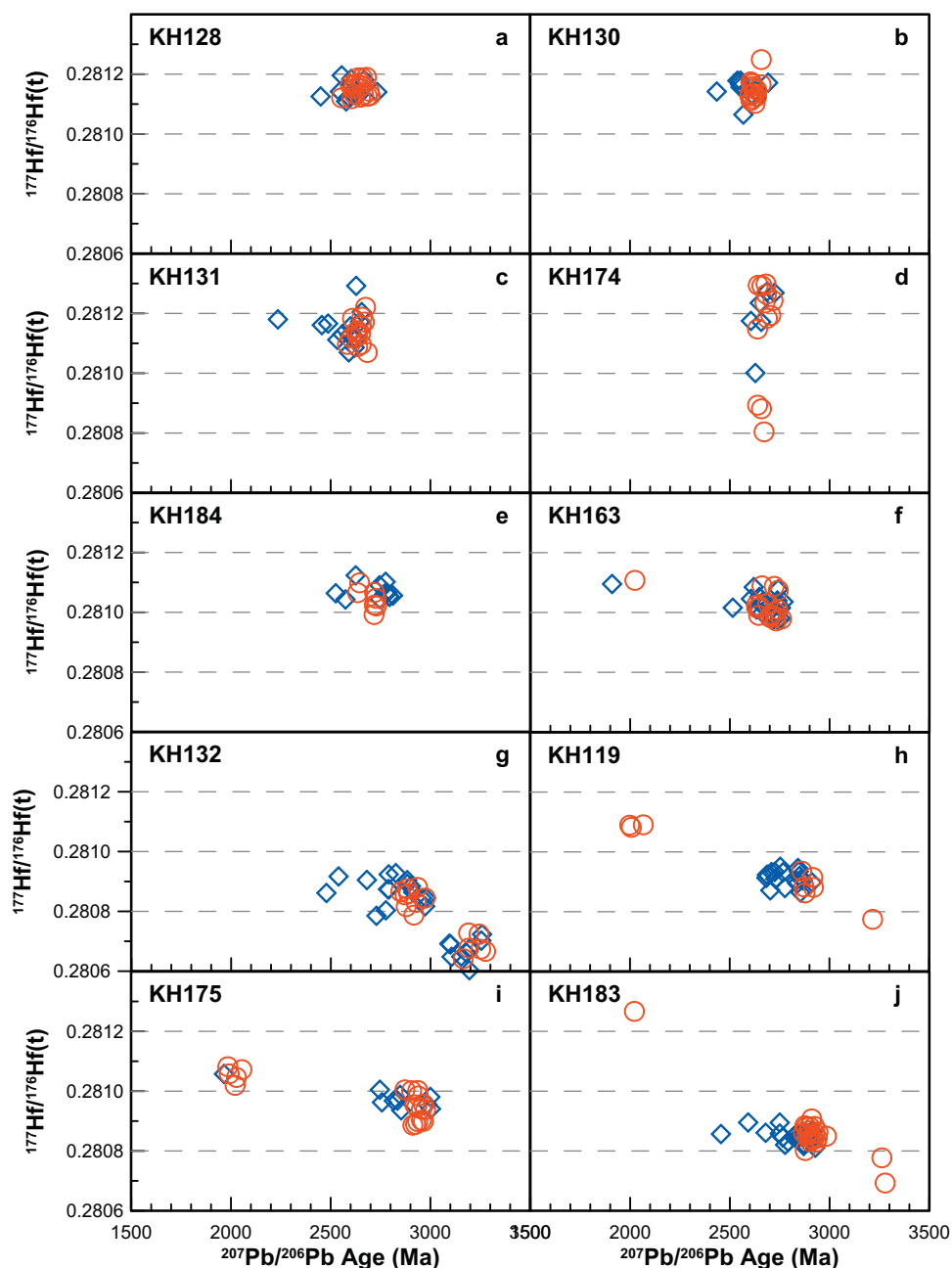
Fig. 7. Variation of initial $^{176}Hf/^{177}Hf$ ratios with apparent $^{207}Pb/^{206}Pb$ ages for zircon analyses of TTG and granitic gneisses from the Kongling terrain. Red circles represent concordant analyses (98–102% concordance level) and blue rhombuses denote discordant analyses. (For interpretation of the references to color in this figure legend, the reader is referred to the web version of this article.)

domains occur as oscillatory zoned cores with thin and structureless rims. The Th/U ratios of all these spots are >0.3 except spot KH132-02 (0.08) (Fig. 5). They give a weighted average age of 3229 ± 42 Ma (n = 7, MSWD = 2.5), which is identical to the upper intercept age of 3231 ± 34 Ma (n = 16, MSWD = 2.4) formed by 9 discordant analyses and the 7 concordant analyses (Fig. 9c).

(2) 2.8–2.9 Ga, which is denoted by 9 concordant age analyses with apparent $^{207}Pb/^{206}Pb$ ages ranging from 2850 Ma to 2973 Ma (Appendix Table 1). These zircon domains occur as cores and show oscillatory zoning patterns with thin and structureless rims (Fig. 8c). All their Th/U ratios are >0.3 (Fig. 5). They, along with 22 discordant analyses, give an upper intercept age of 2901 ± 27 Ma (n = 31, MSWD = 4.3), which is identical to

the weighted average age of 2904 ± 31 Ma (n = 9, MSWD = 1.6) yielded by the 9 concordant analyses (Fig. 9c).

The formation age of this sample can be interpreted in two scenarios. First, the ~3.2 Ga zircon cores were inherited or captured, so the magma intrusion happened at ~2.9 Ga. Alternatively, this gneiss have a migmatitic genesis, and so the ~3.2 Ga and ~2.9 Ga represented two ages of distinct magmatic events. No matter which scenario is chosen, the ~3.2 Ga and the ~2.9 Ga zircons represent two different magmatic events.

Forty Lu-Hf analytical results (Appendix Table 2) reveal that the 3.1–3.2 Ga zircon spots have relatively homogeneous initial $^{176}Hf/^{177}Hf$ ratios of 0.280603–0.280728 and the 2.8–2.9 Ga zircon domains have initial $^{176}Hf/^{177}Hf$ ratios between 0.280785 and
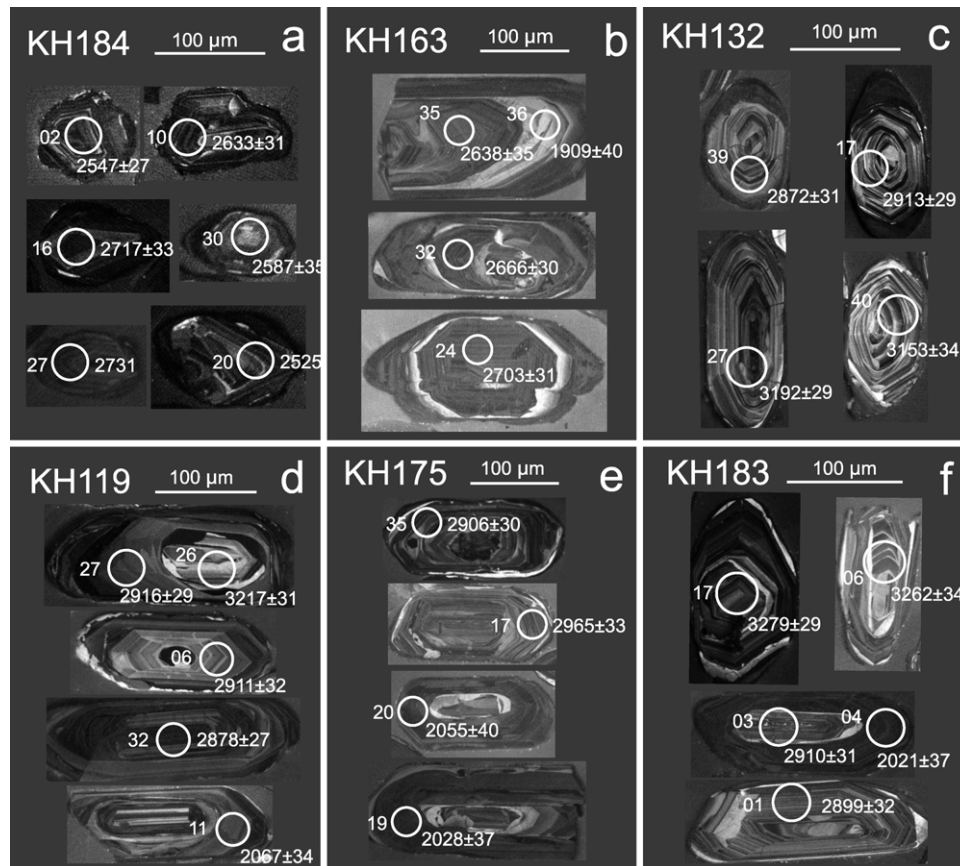
Fig. 8. Typical cathodoluminescence images of zircons for samples KH184 (a), KH163 (b), KH132 (c), KH119 (d), KH175 (e) and KH183 (f) from the Kongling terrain. White circles (32 μm) indicate position of laser spots. Numbers on the left and right side of each spot indicate analytical number and the Pb–Pb age with 1σ error (in Ma).

0.280928 (Fig. 7g), which provide evidence that the two zircon groups were crystallized in two distinct magmatic events. The $\varepsilon_{Hf}(t)$ values of the older zircon cores vary from −3.87 to 0.57 and their T_{DM2} from 3467 to 3695 Ma (Appendix Table 2). In contrast, slightly lower $\varepsilon_{Hf}(t)$ (−5.04 to 0.05) and T_{DM2} (3251–3529 Ma) were obtained from the younger zircon domains (Appendix Table 2).

4.2.3. Trondhjemitic gneisses
4.2.3.1. KH119. For this sample, 50 U–Pb dating analyses were conducted (Appendix Table 1). CL images of most zircon grains show a core-mantle-rim structure (Fig. 8d). Accordingly, three age groups can be distinguished, as shown in Fig. 9d:

(1) 3.2 Ga, which is represented by one concordant zircon core analysis (KH119-26) with $^{207}Pb/^{206}Pb$ age of 3217 ± 31 Ma. The core is characterized by weak oscillatory zoning pattern (Fig. 8d) with Th/U ratio of 0.49 (Fig. 5). We suggest that this old core was captured or inherited and its age may reflect the time of an ancient magmatic event.
(2) 2.8–2.9 Ga, which is represented by 9 concordant analyses with $^{207}Pb/^{206}Pb$ ages ranging from 2861 to 2980 Ma. Some of the zircon crystals are characterized by clear oscillatory zoning patterns, while others are weakly zoned or structureless (Fig. 8d). The Th/U ratios of these spots range from 0.05 to 0.57 with an average of 0.35 (Fig. 5). These concordant analyses yield a weighted average $^{207}Pb/^{206}Pb$ age of 2909 ± 30 Ma (n = 9, MSWD = 1.9), which is, within error, identical to the upper intercept age of 2932 ± 29 Ma (n = 25, MSWD = 1.3) obtained from three rim analyses, 13 discordant mantle ages and the 9 concordant mantle ages (Fig. 9d). Thus the concordant age of

2909 ± 30 Ma for sample KH119 is interpreted as the time of the protolith intrusion.
(3) 2.0 Ga, which is denoted by three concordant U–Pb analyses with $^{207}Pb/^{206}Pb$ age of 1998–2067 Ma. They yield a weighted average of 2023 ± 38 Ma (n = 3, MSWD = 1.2), similar to the lower intercept age of 2039 ± 40 Ma (n = 25, MSWD = 1.3) (Fig. 9d). All of them occur as weakly zoned or structureless rims (Fig. 8d) and their Th/U ratios are of 0.07–0.24 (Fig. 5). This age is interpreted as the time of a Paleoproterozoic metamorphic thermal event.

Twenty-eight Lu–Hf isotope analyses were obtained (Appendix Table 2). For the zircon mantle domains, 24 Lu-Hf analyses yielded relatively similar initial $^{176}Hf/^{177}Hf$ ratios from 0.280863 to 0.280950 (Fig. 7h). They yielded $\varepsilon_{Hf}(t)$ values between −2.09 and 0.95 and T_{DM2} values of 3214–3388 Ma (Appendix Table 2). A relatively lower initial $^{176}Hf/^{177}Hf$ ratio (0.280774) was obtained from the older core and three relatively higher values (0.281082–0.281091) were obtained from the concordant younger rims (Fig. 7h). The $\varepsilon_{Hf}(t)$ value of the older core is 1.96 and its T_{DM2} value is 3392 Ma, whereas the $\varepsilon_{Hf}(t)$ values of the younger rims are between −14.36 and −14.70, with T_{DM2} values of 3209–3243 Ma (Appendix Table 2).

4.2.3.2. KH175. A total of 35 U-Pb dating analyses were obtained (Appendix Table 1). CL images of most the zircons display a core–rim structure (Fig. 8e). Two age populations can be distinguished for the core and rim domains, as shown in Fig. 9e:

(1) 2.8–2.9 Ga, which is represented by 15 concordant U-Pb analyses with apparent $^{207}Pb/^{206}Pb$ ages of 2872–2976 Ma. CL images
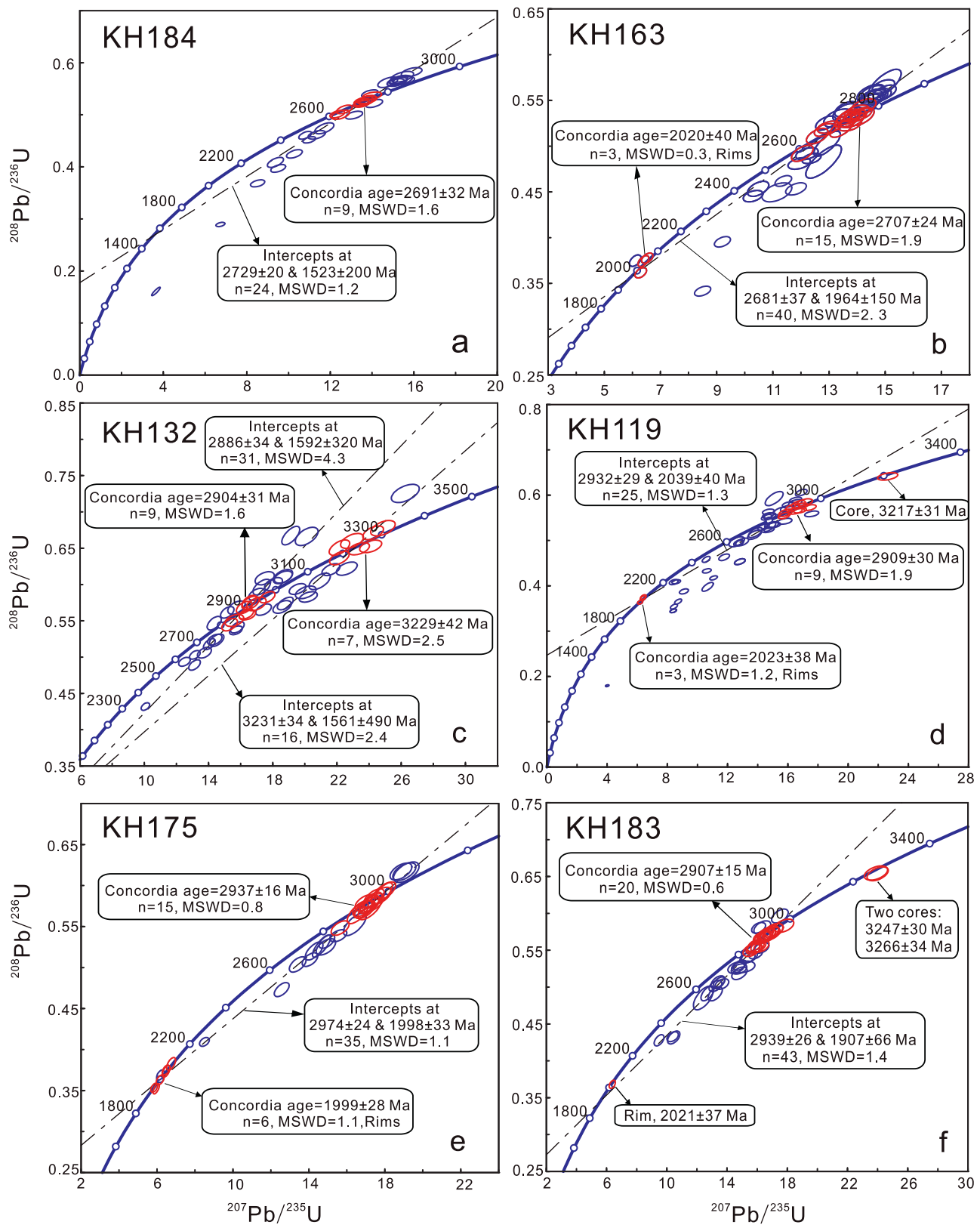
Fig. 9. Zircon U–Pb concordia plots for samples KH184 (a), KH163 (b), KH132 (c), KH119 (d), KH175 (e) and KH183 (f) the Kongling terrain. Red and blue ellipses indicate concordant and discordant analyses, respectively. Errors are ±1σ. (For interpretation of the references to color in this figure legend, the reader is referred to the web version of this article.)

Table 3
Sr–Nd sotopic compositions of rocks from Kongling terrain.

Sample	$^{87}Sr/^{86}Sr$	2σ	$^{87}Rb/^{86}Sr$	$^{143}Nd/^{144}Nd$	2σ	$^{147}Sm/^{144}Nd$	Age (Ma)	T_{DM1} (Ga)	T_{DM2} (Ga)	$\varepsilon_{Nd}(0)$	$\varepsilon_{Nd}(t)$
KH119	0.710754	5	0.171639	0.510393	7	0.07523	2909	3.01	3.05	−43.8	1.59
KH128	0.917031	7	4.685439	0.510943	2	0.10190	2645	2.99	3.01	−33.1	−0.74
KH128(R)	0.917028	5		0.510938	4						
KH130	0.782362	6	1.859029	0.51067	7	0.08160	2622	2.84	2.89	−38.4	0.87
KH131	0.864533	4	2.390731	0.510962	7	0.10688	2640	3.10	3.11	−32.7	−2.08
KH132	0.739135	4	2.330610	0.510585	3	0.09940	2904	3.39	3.43	−40.0	−3.74
KH163	0.711402	4	1.122387	0.510827	7	0.09357	2707	2.93	2.97	−35.3	−0.16
KH174	0.802395	6	0.230129	0.510939	6	0.10171	2671	2.99	3.01	−33.1	−0.75
KH175	0.725807	5	0.461164	0.51056	2	0.08766	2937	3.11	3.15	−40.5	0.19
KH183	0.711203	5	0.205570	0.51072	4	0.10421	2907	3.36	3.37	−37.4	−2.89
KH184	0.759538	5	1.222160	0.511046	3	0.11026	2691	3.08	3.07	−31.1	−1.59

T_{DM2} and $\varepsilon_{Nd}(t)$ were calculated using the respective sample crystallization age. R denotes repeated analysis.

of most cores display oscillatory zoning patterns and some of them are weakly zoned or completely structureless (Fig. 8e). The Th/U ratios of these concordant spots are >0.27 (Fig. 5). They yield a weighted average $^{207}Pb/^{206}Pb$ age of 2937 ± 16 Ma (n = 15, MSWD = 0.8), which is, within error, identical to or slightly younger than the upper intercept age of 2974 ± 24 Ma (n = 35, MSWD = 1.1) given by the 7 rim and 13 discordant and the 15 concordant core analyses (Fig. 9e). This concordant age of 2937 ± 16 Ma is interpreted as the crystallization age of the sample.

(2) 1.9–2.0 Ga, which is denoted by six concordant analyses with apparent $^{207}Pb/^{206}Pb$ ages between 1950 Ma and 2055 Ma. All of them occur as rims and are weakly zoned or structureless (Fig. 8e). Their Th/U ratios are of 0.08–0.21 (Fig. 5). They give a weighted average of 1999 ± 28 Ma (n = 6, MSWD = 1.1) (Appendix Table 1). This concordant age is similar to the lower intercept age of 1998 ± 33 Ma (n = 35, MSWD = 1.1) (Fig. 9e).

Twenty-three Lu–Hf analyses of zircon cores yield initial $^{176}Hf/^{177}Hf$ ratios between 0.280886 and 0.281005 (Appendix Table 2 and Fig. 7i). The $\varepsilon_{Hf}(t)$ values are between −0.60 and 3.55 and their T_{DM2} values are of 3086–3296 Ma (Appendix Table 2). Relatively higher initial $^{176}Hf/^{177}Hf$ ratios (0.281019–0.281072) were obtained for the rim analyses. Their $\varepsilon_{Hf}(t)$ and T_{DM2} values are between −17.46 and −15.25 and between 3246 and 3348 Ma (Appendix Table 2).

4.2.3.3. KH183. Forty-five zircon spots from this sample were carried out for U–Pb dating (Appendix Table 1). CL images of most zircons are characterized by a core–mantle–rim structure (Fig. 8f). However, the cores are usually very small and the rims are very thin (Fig. 8f). Three age populations can be divided for the core, mantle and rim domains, respectively (Fig. 9f):

(1) 3.2 Ga, which is represented by two concordant core analyses with apparent $^{207}Pb/^{206}Pb$ ages of 3266 ± 34 Ma (KH183-06) and 3247 ± 30 Ma (KH183-17). They are characterized by apparent oscillatory zoning (Fig. 8f) and their Th/U ratios are 0.58 and 0.40 (Fig. 5). They are interpreted as inherited or captured.

(2) 2.8–2.9 Ga, which is denoted by 20 concordant analyses with apparent $^{207}Pb/^{206}Pb$ ages between 2861 Ma and 2984 Ma (Appendix Table 1). Most of these zircon domains are clearly oscillatory zoned (Fig. 8f) and their Th/U ratios range from 0.28 to 1.10 with an average of 0.51 (Fig. 5). These age spots, plus one concordant rim analysis and 22 discordant mantle analyses, form a discordia line with an upper intercept age of 2939 ± 26 Ma (n = 43, MSWD = 1.4) which is, within error, identical with the weighted average $^{207}Pb/^{206}Pb$ age of

2907 ± 15 Ma (n = 20, MSWD = 0.6) obtained from the 20 concordant analyses (Fig. 9f). This concordant age is interpreted as the emplacement age of the trondhjemitic magma.

(3) 2.0 Ga, which is represented by only one concordant rim analysis with apparent $^{207}Pb/^{206}Pb$ age of 2021 ± 37 Ma (Appendix Table 1). It is clearly oscillatory zoned with Th/U ratio of 0.09 (Figs. 5 and 8f). This concordant age is similar to or slightly older than the lower intercept age of 1907 ± 66 Ma (n = 43, MSWD = 1.4) (Fig. 9f). The concordant age is interpreted as a Paleoproterozoic metamorphic age.

Forty-two spots were analyzed for Lu–Hf isotope compositions (Appendix Table 2). The initial $^{176}Hf/^{177}Hf(t)$ ratios of the two oldest cores are 0.280693 and 0.280777 and their $\varepsilon_{Hf}(t)$ values are 0.51 and 3.12 with T_{DM2} values of 3513 and 3373 Ma (Appendix Table 2). The Lu–Hf analytical results of 39 spots for the mantle domains reveal homogeneous initial $^{176}Hf/^{177}Hf$ ratios between 0.280801 and 0.280907 (Fig. 7j). Their $\varepsilon_{Hf}(t)$ values vary from −4.32 to −0.54 and T_{DM2} values are 3260–3492 Ma (Appendix Table 2). In contrast, the younger rim gives a relatively higher initial $^{176}Hf/^{177}Hf$ ratio of 0.281267 and its $\varepsilon_{Hf}(t)$ value is −8.17 with T_{DM2} of 2916 Ma (Appendix Table 2).

4.3. Sr–Nd isotopic compositions

Whole rock Sr–Nd isotopic compositions of the 10 gneiss samples were listed in Table 3. Their $\varepsilon_{Nd}(t)$ values and initial Sr isotope compositions were calculated based on their formation ages. As described below, samples KH119, KH132, KH175 and KH183 have formation ages of ~2.9 Ga. Their $\varepsilon_{Nd}(t)$ values are 1.59, −3.74, 0.19 and −2.89, respectively. Their T_{DM2} values vary from 3.05 to 3.43 Ga (Table 3). The other samples show formation ages of ~2.6–2.7 Ga. Their $\varepsilon_{Nd}(t)$ values range from −2.08 to 0.87 with T_{DM2} values of 2.84–3.08 Ga (Table 3).

5. Discussion

5.1. Zircon genesis from the combination of U–Pb and Lu–Hf systematics

Zircon CL images, Th/U ratios and U–Pb ages are the general methods to distinguish zircon growth from alteration. However, none of these methods can offer unambiguous interpretation on the age implication for the following two reasons. First of all, although the Th/U ratios of igneous zircons are usually higher than those of metamorphic zircons, there is no apparent boundary value between them. Then, owing to subsequent Pb loss, zircon domains formed during the same event may yield a wide scatter of U–Pb ages. This makes the selection of certain zircon domains,

when a discordia line is calculated, more ambiguous and difficult. In this study, we use the combined set of CL images, Th/U ratios, U–Pb ages and Lu–Hf isotopic compositions to conquer this problem.

The Lu–Hf system of zircon is more resistant to the change of external conditions than the U–Pb system and thus in many cases, the U–Pb system was perturbed but the Lu–Hf system was able to keep pristine (Patchett, 1983; Kinny et al., 1991; Kinny and Maas, 2003; Gerdes and Zeh, 2009). In general, three scenarios can be observed in this study. In the first case, zircon domains of individual samples yield, within error, identical $^{207}Pb/^{206}Pb$ ages and initial $^{176}Hf/^{177}Hf$ ratios. This case was observed from samples KH128, KH130, KH131, KH184 and KH163 (Fig. 7a–c, e and f). Additionally, most of the zircon CL images from the first three samples reveal igneous oscillatory zoning patterns, although some complex structures cannot be excluded, and their Th/U ratios are usually higher than 0.3 (Fig. 5). All these lines of evidence indicate that these zircon domains were, undoubtedly, crystallized from the same magma (Rubatto, 2002; Corfu et al., 2003; Hoskin and Schaltegger, 2003). However, the situation for sample KH163 and KH184 is more complex than samples KH128, KH130 and KH131. The two samples will be discussed below.

In the second case, some zircons reveal relatively identical $^{207}Pb/^{206}Pb$ ages but show a wide scatter of initial $^{176}Hf/^{177}Hf$ ratios over ±0.0001. This case was only observed in sample KH174 (Fig. 7d). Zeh et al. (2009) considered that this phenomenon was caused by crystallization within a short time interval from the same magma, which yield a heterogeneous Hf isotopic composition. Because nearly all analyzed zircon domains yield relatively identical $^{207}Pb/^{206}Pb$ ages, the U–Pb system, which is easier to be disturbed than the Lu–Hf system, is still pristine, indicating the wide range of initial $^{176}Hf/^{177}Hf$ ratios was not caused by post growth or alteration. Another possibility is source heterogeneity. Most analyzed zircon domains in this sample have, within error, identical $^{207}Pb/^{206}Pb$ ages and initial $^{176}Hf/^{177}Hf$ ratios to samples KH128, KH130 and KH131. Moreover, these four samples have similar major and trace element compositions (Figs. 2 and 3). Consequently, they might record the same magmatic event.

In the third case, zircon domains crystallized from the same magma have, within error, identical initial $^{176}Hf/^{177}Hf$ ratios but yield a wide range of their corresponding $^{207}Pb/^{206}Pb$ ages resulting from various Pb loss via alteration (Amelin et al., 2000; Gerdes and Zeh, 2009; Zeh et al., 2009). This is reflected by relatively horizontal arrays in the $^{207}Pb/^{206}Pb$ age vs $^{176}Hf/^{177}Hf(t)$ plots and was observed in samples KH132, KH119, KH175 and KH183 (Fig. 7g–j). For zircon cores, they have lower initial $^{176}Hf/^{177}Hf$ ratios and older $^{207}Pb/^{206}Pb$ ages and thus plot in the right bottom of the $^{207}Pb/^{206}Pb$ age vs $^{176}Hf/^{177}Hf(t)$ plots (KH132, KH119 and KH183) (Fig. 7g, h and j). Additionally, nearly all these cores display apparent oscillatory zoning patterns (Fig. 8c, d and f) and have high Th/U ratios (usually >0.3) (Fig. 5). All these features suggest that these older cores were formed in an older magmatic event (Rubatto, 2002; Corfu et al., 2003; Hoskin and Schaltegger, 2003). The zircon rims often yield higher initial $^{176}Hf/^{177}Hf$ ratios and younger $^{207}Pb/^{206}Pb$ ages and thus plot in the upper left of the $^{207}Pb/^{206}Pb$ age vs $^{176}Hf/^{177}Hf(t)$ plots (KH119, KH175 and KH183) (Fig. 7h–j). They are generally complex or structureless in the CL images (Fig. 8b and d–f) and have lower Th/U ratios (often <0.3) (Fig. 5), indicative metamorphic genesis. The zircon mantles of these four samples generally display apparently magmatic oscillatory zoning patterns in CL images and evaluated Th/U ratios (>0.3) (Fig. 5). Besides, they have identical $^{207}Pb/^{206}Pb$ ages and similar intermediate initial $^{176}Hf/^{177}Hf$ ratios (Fig. 7g–j), inferring that these zircon domains record another magmatic event.
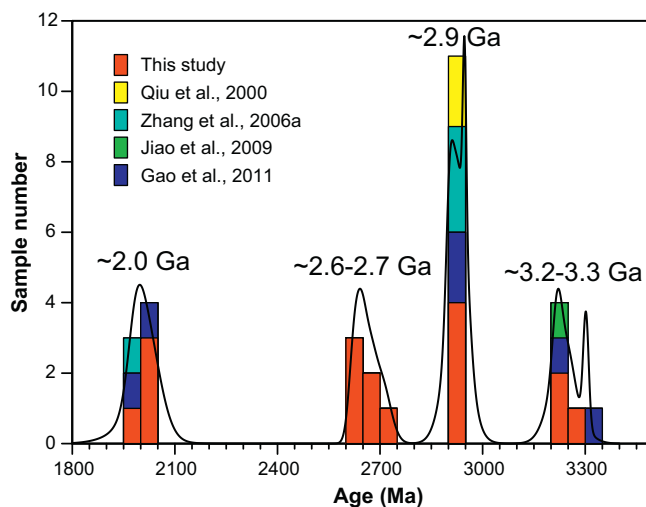

Fig. 10. Cumulative probability plot of zircon crystallization ages of TTG and granitic gneisses from the Kongling terrain in this study and previous studies (Qiu et al., 2000; Zhang et al., 2006a; Jiao et al., 2009; Gao et al., 2011).

5.2. Three Archean magmatic events

5.2.1. ~2.6–2.7 Ga A-type granites

Early at the end of the last century, Ling et al. (1998) acquired two whole rock Sm–Nd isochron ages of 2742 ± 83 Ma and 2728 ± 118 Ma for an amphibolite and a TTG gneiss from the Kongling terrain. However, the obtained ages have very large errors. Based on in situ zircon U–Pb dating, a couple of near concordant zircons from TTG gneisses with ages around ~2.6–2.7 Ga were obtained in the North Kongling terrain and these ages were interpreted as metamorphic ages (Qiu et al., 2000; Jiao et al., 2009; Gao et al., 2011). Zheng et al. (2006) reported several ~2.6 Ga zircon xenocrysts in Jingshan (2614 Ma) and Zhenyuan (2632 Ma) lower crustal xenoliths from the Yangtze craton. Thus, a wide spread Archean basement was speculated beneath Yangtze craton. Detrital zircons of this age were also found from metapelites and Neoproterozoic sediments (Liu et al., 2008a; Gao et al., 2011). However, none of these studies provide unambiguous evidence for a ~2.6–2.7 Ga magmatic event.

The present study reports, for the first time, clear magmatic ~2.6–2.7 Ga zircon ages for four orthogneisses (KH128, KH130, KH131 and KH174) in the eastern segment of the North Kongling terrain (Fig. 10). Most of the concordant zircons are apparently or weakly oscillatory zoned (Fig. 4a–d) and their Th/U ratios are above 0.3 (Fig. 5). Besides, they have relatively homogeneous initial $^{176}Hf/^{177}Hf$ ratios and similar concordant ages of 2622–2707 Ma (Fig. 6a–d). It is concluded that these ages represent the intrusion age of a late Archean magmatism.

Apart from the similarity mentioned above, these four samples also possess A-type granites affinity. They show relatively high REE (530–1074 ppm), apparently negative Eu anomaly (Eu/Eu* = 0.22–0.35), low #Mg (19.51–22.63) (molar $100 \times Mg/(Mg + Fe)$) and low La_N/Yb_N (10.3–24.2) (Fig. 3a). They are intensively depleted in Sr–Eu–Ti and weakly depleted in Nb and Ta (Fig. 3b). Besides, they have high K-feldspar proportion (about 45–60%) and relatively evaluated $(K_2O + Na_2O)/CaO$, TFeO/MgO, Zr, Nb, Ce and Y contents (Fig. 11). Their $10,000 \times Ga/Al$ ratios range between 3.00 and 3.54 (Fig. 11). In the discrimination diagrams of $(K_2O + Na_2O)/CaO$, TFeO/MgO, Zr, Nb, Ce and Y vs $10,000 \times Ga/Al$ ratios, they all plot in the A-type granites field, proposed by Whalen et al. (1987) (Fig. 11). All these features suggest that the protoliths of these four gneisses are A-type granites (Loiselle and Wones, 1979; Collins et al., 1982; Whalen et al., 1987; Eby, 1990; King et al., 2001;
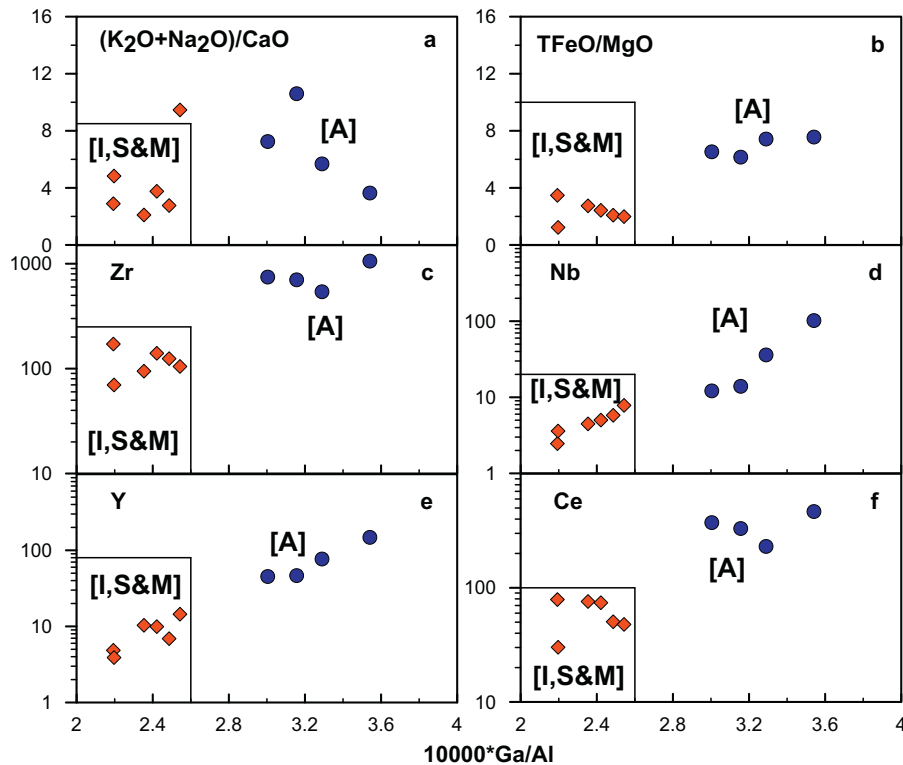
Fig. 11. (a) ($K_2O + Na_2O$)/CaO, (b) (TFeO/MgO), (c) Zr, (d) Nb, (e) Y and (f) Ce vs. 10,000 Ga/Al discrimination diagrams of the Kongling gneisses (Whalen et al., 1987). Blue circles represent sample KH128, KH130, KH132 and KH174. Red rhombuses denote other samples. [A], A-type granites; [I, S and M], I-type, S-type and M-type granites. (For interpretation of the references to color in this figure legend, the reader is referred to the web version of this article.)

Bonin, 2007). Thus, the present study reports, also for the first time, the occurrence of Archean A-type granites in the Yangtze craton. The other six samples, on the other hand, plot in the I, S & M-type granite field (Fig. 11).

Like the four ~2.6–2.7 Ga A-type granites mentioned above, two other samples (KH184 and KH163) have crystallization ages of ~2.6–2.7 Ga, too. However, geochemical and isotopic evidence suggest that they are apparently different from the A-type granites. The ~2.6–2.7 Ga zircon $\varepsilon_{Hf}(t)$ values of these two samples (−14.49 to 2.08) are relatively lower than those of the four A-type granites. The zircons of sample KH184 are relatively smaller (50–100 μm) than those from other samples (Fig. 8a). They have high Th (100–350 ppm) and U (1000–6000 ppm) contents and low Th/U ratios (0.01–0.17) (Appendix Table 1). Some CL images reveal oscillatory zoning patterns and some are structureless (Fig. 8a). In addition, sample KH184 has similar trace element features with the ~2.9 Ga TTGs (Fig. 3a and b). Hence, the protolith of this sample might be country rock (~2.9 Ga TTG) of the ~2.6–2.7 Ga magmatism and these zircons were seriously modified and perturbed by the ~2.6–2.7 Ga magmatism. As for sample KH163, it also has parallel trace element characteristics to the ~2.9 Ga TTGs (Fig. 3a and b). Therefore, it is possible that zircons in this sample recrystallized from the ~2.9 Ga zircons when the ~2.6–2.7 Ga magma emplaced.

5.2.2. 2.9 Ga magmatism

This magmatism was first reported as trondhjemitic emplacement at 2.90–2.95 Ga in the western segment of the North Kongling terrain by Qiu et al. (2000) and then was further confirmed by Zhang et al. (2006c). Zhang et al. (2006c) considered this magmatic event formed the major part of the whole Kongling terrain. Recently, Gao et al. (2011) reported a magmatic event of the same age in the South Kongling terrain and supported that the ~2.9 Ga magmatism produced rocks dominating the whole Kongling terrain. The ~2.9 Ga igneous zircons are also abundant in Precambrian

sedimentary rocks from the Kongling area (Qiu et al., 2000; Zhang et al., 2006b; Liu et al., 2008a; Gao et al., 2011). However, these studies do not cover the eastern part of the Kongling terrain. It remains uncertain whether this magmatism is dominant in the eastern part of the North Kongling terrain.

As described above, three TTG gneisses (KH119, KH175 and KH183) and a granitic gneiss (KH132) dated from the eastern segment have emplacement ages of ~2.90–2.95 Ga (Fig. 9c–f). The concordant 2.9 Ga zircons in these samples exhibit apparent oscillatory zoning patterns in the cores with very thin rims (Fig. 8c–f) and have Th/U ratios >0.3 (Fig. 5), typical of igneous zircons. The results indicate that the ~2.9 Ga magmatism was also abundant in the eastern segment of the North Kongling terrain. Taking all the available age datasets (Fig. 10) into consideration (Qiu et al., 2000; Zhang et al., 2006a; Jiao et al., 2009; Gao et al., 2011), nearly all segments of the whole Kongling terrain experienced the magmatic event of ~2.9 Ga. Thus, it is now reasonable to conclude that the major part of the Kongling terrain was produced by the ~2.9 Ga magmatism. Nevertheless, owing to the limited data, it is still vague that whether this magmatism lasted from 2.90 to 2.95 Ga or occurred as two or more episodic events. Apart from the Kongling terrain, ~2.9 Ga igneous zircons are also reported in other nearby areas in South China, such as Huangtuling in the northern Dabie Orogen (Sun et al., 2008; Wu et al., 2008b) and Ningxiang (Zheng et al., 2006), which may reflect the presence of widespread Mesoarchean basement beneath the Yangtze craton.

5.2.3. ~3.2–3.3 Ga magmatism

The first evidence of >3.2 Ga zircons in the Kongling terrain was reported by Qiu et al. (2000) and ~3.5–3.8 Ga zircons were subsequently observed in Neoproterozoic sediments along the southern margin of the Kongling terrain (Zhang et al., 2006b; Liu et al., 2008a). However, these ages were all obtained from detrital zircons and thus their origin was ambiguous. The first evidence of >3.2 Ga

Table 4
Compilation of zircon U–Pb ages of TTG and granitic gneisses in the Kongling terrain.

Locality		Sample	Rock type	Age (Ma)	1σ	Origin	T_{DM2}	Method	Reference
North Kongling terrain	Eastern part	KH119	Trondhjemite gneiss	2908	21	Magmatic	3.2–3.3 Ga	LA-ICP-MS	This study
				3233	32	Magmatic			
				2007	48	Metamorphic			
		KH128	Granitic gneiss	2640	17	Magmatic	2.9–3.0 Ga		
		KH130	Granitic gneiss	2636	19	Magmatic	2.9–3.1 Ga		
		KH131	Granitic gneiss	2601	29	Magmatic	2.7–3.0 Ga		
		KH132	Granitic gneiss	2901	27	Magmatic	3.2–3.7 Ga		
				3231	34	Magmatic			
		KH163	Trondhjemite gneiss	2733	20	Magmatic	3.0–3.2 Ga		
				2023	51	Metamorphic			
		KH174	Granitic gneiss	2652	22	Magmatic	2.7–3.5 Ga		
		KH175	Tonalitic gneiss	2957	17	Magmatic	3.1–3.3 Ga		
				1995	45	Metamorphic			
		KH183	Trondhjemite gneiss	2901	18	Magmatic	3.2–3.5 Ga		
				3255	44	Magmatic			
				2021	37	Metamorphic			
		KH184	Granitic gneiss	2735	40	Magmatic	2.9–3.2 Ga		
	Western part	KY05	Trondhjemite gneiss	2947	5	Magmatic	No Hf data	SHRIMP	Qiu et al. (2000)
		KY17	Trondhjemite gneiss	2903	10	Magmatic	No Hf data		
		04YC97	Migmatite	2936	28	Magmatic	3.3–3.7 Ga	LA-ICP-MS	Zhang et al. (2006a)
				1980	72	Metamorphic			
		04YC104	Migmatite	2947	28	Magmatic	3.3–3.6 Ga		
				3242	40	Magmatic			
		KY05	Trondhjemite gneiss	2930	44	Magmatic	3.3–3.6 Ga		
				3182	175	Magmatic			
	Northern margin	06HL09	Gneiss	3218	13	Magmatic	3.4–3.8 Ga	LA-ICP-MS	Jiao et al. (2009)
	Southern margin	KH80	Granodiritic gneiss	3262	27	Magmatic	3.2–3.9 Ga	LA-ICP-MS	Gao et al. (2011)
				1981	16	Metamorphic			
		KH84	Trondhjemite gneiss	3302	8	Magmatic	3.2–3.8 Ga		
South Kongling terrain		KH89	Granodiritic gneiss	2950	15	Magmatic	3.3–3.8 Ga	LA-ICP-MS	Gao et al. (2011)

zircons in TTG gneiss was reported by Zhang et al. (2006a), who identified several zircons with core U–Pb ages around 3.2 Ga in two migmatites and one trondhjemitic gneiss in the western part of the North Kongling terrain. Jiao et al. (2009) reported an intrusion age of 3218 ± 13 Ma for a gneiss at the northeast edge of the Kongling terrain. Gao et al. (2011) obtained a concordant $^{207}Pb/^{206}Pb$ age of 3307 ± 7 (1σ) Ma for a trondhjemitic gneiss (KH84) along the southern margin of the North Kongling terrain. This age was interpreted as the age of the trondhjemitic magmatism, and the gneiss represents the oldest known rock in South China.

In this study, we report 10 concordant zircon cores around 3.2 Ga for three gneisses (KH119, KH132 and KH183) in the eastern part of the North Kongling terrain. Most of these cores are characterized by apparently oscillatory zoning patterns and have Th/U ratios >0.3 (Fig. 5), typical characteristics of igneous zircons. Furthermore, there is an apparent age peak at about 3.2 Ga (Fig. 10). Regardless as inherited or captured, these zircon cores crystallized from magma distinct from their host rocks. The results confirm the existence of late Paleoarchean to early Mesoarchean granitoid magmatism in the Kongling terrain. Taken together, both the western and eastern parts of the North Kongling terrain have ~3.2 Ga igneous zircons, indicating that the scale of the oldest known magmatism is much larger than previously thought. This oldest nucleus of the Yangtze craton might have formed a certain size in the Late Paleoarchean to Early Mesoarchean eon and was reworked by subsequent magmatic or/and metamorphic events.

Apart from the above three magmatic events, four samples (KH163, KH119, KH175 and KH183) yield metamorphic ages of ~2.0 Ga for zircon rims. These age domains are structureless or weakly zoned (Fig. 8b, d–f) and usually have Th/U ratios < 0.3 (Fig. 5), indicative of metamorphic origin. Similar results were also obtained by previous studies in the Kongling terrain (Qiu et al., 2000; Zhang et al., 2006a, c; Wu et al., 2009; Gao et al., 2011). The ~2.0 Ga metamorphic ages are widespread in other areas of the Yangtze craton (Compston et al., 1992; Ayers et al., 2002; Yang et al., 2003; Bryant et al., 2004; Li et al., 2004; Huang et al., 2006),

and was interpreted as a result of orogeny possibly associated with the assembly of the supercontinent Columbia (Zhang et al., 2006c; Wu et al., 2009).

5.3. Crustal growth and reworking

The TTG and granitic gneisses in the Kongling terrain are the oldest rocks found in the Yangtze craton (Zhang et al., 2006a; Jiao et al., 2009; Gao et al., 2011). Consequently, their genesis and evolution is extraordinarily significant for understanding the time of crustal extraction and reworking of South China. A compilation of available concordant zircon ages of TTG and granitic gneisses from this study and previous literature (Qiu et al., 2000; Zhang et al., 2006a; Jiao et al., 2009; Gao et al., 2011) reveals three igneous age peaks in Archean (~3.2–3.3 Ga, ~2.9 Ga and ~2.6–2.7 Ga) and one metamorphic age peak in Paleoproterozoic (~2.0 Ga) (Table 4 and Fig. 10). Hence, the Kongling terrain experienced at least three Archean magmatic events, and one Paleoproterozoic metamorphic event.

Zircons crystallized at ~2.6–2.7 Ga have $\varepsilon_{Hf}(t)$ values ranging from −9.67 up to 7.93 (close to the depleted mantle value) (Fig. 13). Their T_{DM2} values vary from 3514 to 2650 Ma. Of them, 102 zircons have $\varepsilon_{Hf}(t) > 0$ and they account for 65% of the ~2.6–2.7 Ga zircon population, which is significantly greater than those for the two older magmatic events. Although their whole rock $\varepsilon_{Nd}(t)$ are nearly chondritic, previously studies revealed that Nd isotopes of the early Archean gneisses do not faithfully record isotopic variations on the early Earth (e.g. Vervoort et al., 1996). Therefore, our results clearly indicate a considerably higher proportion of new crustal component (about 65% of the whole magma) in the ~2.6–2.7 Ga granitoids compared to the ~3.2–3.3 Ga and ~2.9 Ga TTGs. As a result, most of the ~2.6–2.7 Ga zircons plot significantly above the evolution arrays formed by the two older magmatic events. Our conclusion agree well with age spectra of igneous and detrital zircons from worldwide areas (Rino et al., 2004; Condie and Aster, 2009, 2010; Condie et al., 2009, 2011; Condie and O'Neill, 2009;), which
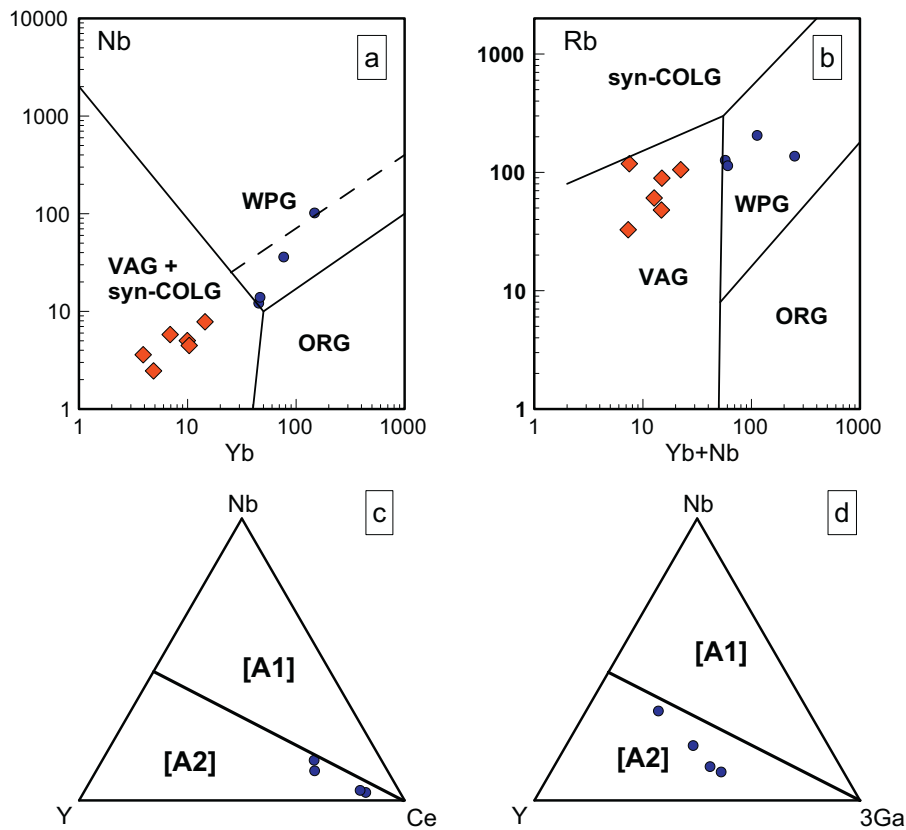
Fig. 12. Diagrams (a) and (b) are Nb vs Y and Rb vs (Y + Nb) of the Kongling gneisses (Pearce et al., 1984). VAG, volcanic arc granites; ORG, ocean ridge granites; WPG, within-plate granites; Syn-COLG and Post-COLG, syn- and post-collision granites. Diagrams (c) and (d) are the A$_1$ and A$_2$ subgroup discriminations of the Kongling terrain A-type granites (Eby, 1992). Blue circles represent sample KH128, KH130, KH132 and KH174. Red rhombuses denote the other samples. (For interpretation of the references to color in this figure legend, the reader is referred to the web version of this article.)

document that several age peaks between 2.65 Ga and 2.76 Ga represent increases in the volume of juvenile continental crust.

There seems to be general agreement that the parental magmas of A-type granites is derived either from partial melting of mafic lower crust or from differentiation of crustally contaminated mantle-derived magma in an extensional environment (Collins et al., 1982; Whalen et al., 1987; Eby, 1990, 1992). Based on the tectonic discrimination diagrams of Nb–Y (Fig. 12a) and Rb–(Y + Nb) (Fig. 12b) (Pearce et al., 1984), the four A-type granites fall into the WPG (within plate granites) field, while the other six samples plot in the VAG (volcanic arc granites) field. In the chemical subdivision diagrams of A-type granitoids (Fig. 12c and d), all the four A-type granites plot in the field of A$_2$, type which represents magmas derived from continental crust or underplated crust (Eby, 1992). However, the models proposed by Eby (1992) presumed that the magmas were derived by partial melting of crustal materials and he also noted that it is not possible, on the base of trace elements, to rule out a subcontinental mantle source for some A-type granites. The ~2.6–2.7 magma in this study contains a large proportion of juvenile materials, and then was contaminated by old crustal components. This was documented by many positive zircon $\varepsilon_{Hf}(t)$ values and a few negative ones (Fig. 13). Consequently, we believe that the ~2.6–2.7 Ga A-type granites formed in a within plate setting and derived from differentiation of magma derived from partial melting of juvenile materials, contaminated by old crustal components.

One hundred and fifteen zircons from the four ~2.9 Ga samples (KH119, KH132, KH175 and KH183) in this study have $\varepsilon_{Hf}(t)$ values ranging from −7.66 to 3.55 and their T_{DM2} values vary between 3086 and 3599 Ma (Appendix Table 2 and Fig. 13). This agrees well
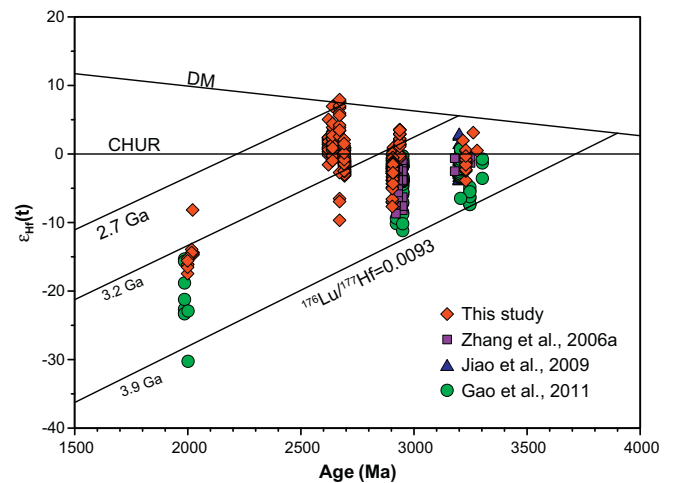
Fig. 13. Variation of zircon Hf isotopes with age for rocks from the Kongling terrain in this study and previous studies (Zhang et al., 2006a; Jiao et al., 2009; Gao et al., 2011). Also shown are evolution trends of depleted mantle (DM), chondritic reservoir (CHUR) and continental crust separated from the depleted mantle at 3.9 Ga, 3.2 Ga and 2.7 Ga with $^{176}Lu/^{177}Hf = 0.0093$ (Vervoort and Patchett, 1996).

with the Sr–Nd isotopic data with the two-stage Nd model ages ranging from 3.05 to 3.43 Ga. Collectively, these results suggest that the ~2.90 Ga TTGs were generated by reworking of older rocks with rare additions of juvenile crust (Fig. 13). The $\varepsilon_{Hf}(t)$ values of the ~3.2 Ga magmatic zircon cores are between −3.87 and 3.12 and their T_{DM2} values vary from 3373 to 3695 Ma with an average of ~3.5 Ga (Appendix Table 2 and Fig. 13). About 70 zircon cores with

ages of ~3.2–3.3 Ga have been obtained in previous and present studies, with $\varepsilon_{Hf}(t)$ values between −7.37 and 3.0 and T_{DM2} values of 3358–3867 Ma (Zhang et al., 2006a; Jiao et al., 2009; Gao et al., 2011). These results suggest that most of these zircon cores crystallized from a magma generated by remelting of an older crust, which was formed between 3.4 and 3.8 Ga. This hints that the ancient crust had been preserved in the crust for ~200–500 Ma and then was remelted to form the ~3.2–3.3 Ga emplacement.

6. Conclusions

Three Archean magmatic events are present in the Kongling terrain, South China at ~2.6–2.7 Ga, ~2.9 Ga and ~3.2–3.3 Ga. The unambiguous ~2.6–2.7 Ga magmatism is our first finding in the Yangtze craton. The majority of the Kongling terrain formed at ~2.9 Ga. The ~3.2–3.3 Ga rocks are sporadically exposed. About 65% of the ~2.6–2.7 Ga zircons have $\varepsilon_{Hf}(t)$ above zero and up to the depleted mantle value. This indicates that they contain a considerably higher proportion of juvenile crustal component. This, in turn, supports worldwide zircon studies that age peaks at 2.65–2.76 Ga represent increases in the volume of juvenile continental crust. The Hf isotopes also suggest that most of the ~3.2–3.3 Ga and ~2.9 Ga zircons were derived from pre-existing crustal rocks with rare juvenile crustal additions.

Acknowledgements

References

Amelin, Y., Lee, D.C., Halliday, A.N., 2000. Early-middle Archaean crustal evolution deduced from Lu–Hf and U–Pb isotopic studies of single zircon grains. Geochimica et Cosmochimica Acta 64, 4205–4225.

Andersen, T., Griffin, W.L., Pearson, N.J., 2002. Crustal evolution in the SW part of the Baltic Shield: the Hf isotope evidence. Journal of Petrology 43, 1725–1747.

Ayers, J.C., Dunkle, S., Gao, S., Miller, C.F., 2002. Constraints on timing of peak and retrograde metamorphism in the Dabie Shan Ultrahigh-Pressure Metamorphic Belt, east-central China, using U–Th–Pb dating of zircon and monazite. Chemical Geology 186, 315–331.

Barker, F., 1979. Trondhjemites: definition, environment and hypothesis of origin. In: Barker, F. (Ed.), Trondhjemites, Dacites and Related Rocks. Elsevier, Amsterdam, pp. 1–12.

Blichert-Toft, J., Chauvel, C., Albarède, F., 1997. Separation of Hf and Lu for high-precision isotope analysis of rock samples by magnetic sector-multiple collector ICP-MS. Contributions to Mineralogy and Petrology 127, 248–260.

Blichert-Toft, J., Albarede, F., 1997. The Lu–Hf isotope geochemistry of chondrites and the evolution of the mantle–crust system. Earth and Planetary Science Letters 148, 243–258.

Bonin, B., 2007. A-type granites and related rocks: evolution of a concept, problems and prospects. Lithos 97, 1–29.

Bryant, D.L., Ayers, J.C., Gao, S., Miller, C.F., Zhang, H.F., 2004. Geochemical, age, and isotopic constraints on the location of the Sino-Korean/Yangtze Suture and evolution of the Northern Dabie Complex, east central China. Geological Society of America Bulletin 116, 698–717.

Chen, J.F., Jahn, B.M., 1998. Crustal evolution of southeastern China: Nd and Sr isotopic evidence. Tectonophysics 284, 101–133.

Chu, N.C., Taylor, R.N., Chavagnac, V., Nesbitt, R.W., Boella, R.M., Milton, J.A., German, C.R., Bayon, G., Burton, K., 2002. Hf isotope ratio analysis using multi-collector inductively coupled plasma mass spectrometry: an evaluation of isobaric interference corrections. Journal of Analytical Atomic Spectrometry 17, 1567–1574.

Collins, W., Beams, S., White, A., Chappell, B., 1982. Nature and origin of A-type granites with particular reference to southeastern Australia. Contributions to Mineralogy and Petrology 80, 189–200.

Compston, W., Williams, I.S., Kirschvink, J.L., Zichao, Z., Guogan, M.A., 1992. Zircon U–Pb ages for the early Cambrian time-scale. Journal of the Geological Society 149, 171–184.

Condie, K.C., 1981. Archaean Greenstone Belts. Elsevier, Amsterdam, p. 434.

Condie, K.C., 2005. TTGs and adakites: are they both slab melts? Lithos 80, 33–44.

Condie, K.C., Aster, R.C., 2009. Zircon age episodicity and growth of continental crust. Eos Trans. AGU 90, 364–365.

Condie, K.C., Belousova, E., Griffin, W.L., Sircombe, K.N., 2009. Granitoid events in space and time: constraints from igneous and detrital zircon age spectra. Gondwana Research 15, 228–242.

Condie, K.C., O'Neill, C., 2009. A new perspective on the 2.7 Ga event on Earth. Geochimica et Cosmochimica Acta 73, A240.

Condie, K.C., Aster, R.C., 2010. Episodic zircon age spectra of orogenic granitoids: the supercontinent connection and continental growth. Precambrian Research 180, 227–236.

Condie, K.C., Bickford, M.E., Aster, R.C., Belousova, E., Scholl, D.W., 2011. Episodic zircon ages, Hf isotopic composition, and the preservation rate of continental crust. Geological Society of America Bulletin 123, 951–957.

Corfu, F., Hanchar, J.M., Hoskin, P.W.O., Kinny, P., 2003. Atlas of zircon textures. In: Hanchar, J.M., Hoskin, P.W.O. (Eds.), Zircon. The Geological Society of America, Washington, USA, pp. 469–500.

Davis, D.W., Amelin, Y., Nowell, G.M., Parrish, R.R., 2005. Hf isotopes in zircon from the western superior province, Canada: implications for Archean crustal development and evolution of the depleted mantle reservoir. Precambrian Research 140, 132–156.

Drummond, M.S., Defant, M.J., 1990. A model for trondhjemite-tonalite-dacite genesis and crustal growth via slab melting: Archean to modern comparisons. Journal of Geophysical Research – Solid Earth and Planets 95, 21503–21521.

Eby, G.N., 1990. The A-type granitoids: a review of their occurrence and chemical characteristics and speculations on their petrogenesis. Lithos 26, 115–134.

Eby, G.N., 1992. Chemical subdivision of the A-type granitoids: petrogenetic and tectonic implications. Geology 20, 641–644.

Elhlou, S., Belousova, E., Griffin, W.L., Pearson, N.J., O'Reilly, S.Y., 2006. Trace element and isotopic composition of GJ-red zircon standard by laser ablation. Geochimica et Cosmochimica Acta 70, A158.

Gao, S., Zhang, B.R., 1990. The discovery of Archean TTG gneisses in northern Yangtze craton and their implications. Earth Science 15, 675–679 (in Chinese with English abstract).

Gao, S., Ling, W.L., Qiu, Y.M., Lian, Z., Hartmann, G., Simon, K., 1999. Contrasting geochemical and Sm–Nd isotopic compositions of Archean metasediments from the Kongling high-grade terrain of the Yangtze craton: evidence for cratonic evolution and redistribution of REE during crustal anatexis. Geochimica et Cosmochimica Acta 63, 2071–2088.

Gao, S., Rudnick, R.L., Yuan, H.L., Liu, X.M., Liu, Y.S., Xu, W.L., Ling, W.L., Ayers, J., Wang, X.C., Wang, Q.H., 2004. Recycling lower continental crust in the North China craton. Nature 432, 892–897.

Gao, S., Yang, J., Zhou, L., Li, M., Hu, Z.C., Guo, J.L., Yuan, H.L., Gong, H.J., Xiao, G.Q., Wei, J.Q., 2011. Age and growth of the Archean Kongling terrain, South China, with emphasis on 3.3 Ga granitoid gneisses. American Journal of science 311, 153–182.

Geng, Y., Du, L., Ren, L., 2012. Growth and reworking of the early Precambrian continental crust in the North China Craton: Constraints from zircon Hf isotopes. Gondwana Research 21, 517–529.

Gerdes, A., Zeh, A., 2009. Zircon formation versus zircon alteration—new insights from combined U–Pb and Lu–Hf in-situ LA-ICP-MS analyses, and consequences for the interpretation of Archean zircon from the Central Zone of the Limpopo Belt. Chemical Geology 261, 230–243.

Griffin, W.L., Pearson, N.J., Belousova, E., Jackson, S.E., van Achterbergh, E., O'Reilly, S.Y., Shee, S.R., 2000. The Hf isotope composition of cratonic mantle: LAM-MC-ICPMS analysis of zircon megacrysts in kimberlites. Geochimica et Cosmochimica Acta 64, 133–147.

Griffin, W.L., Belousova, E.A., Shee, S.R., Pearson, N.J., O'Reilly, S.Y., 2004. Archean crustal evolution in the northern Yilgam Craton: U–Pb and Hf-isotope evidence from detrital zircons. Precambrian Research 131, 231–282.

Griffin, W.L., Pearson, N.J., Belousova, E.A., Saeed, A., 2006. Comment: Hf-isotope heterogeneity in zircon 91500. Chemical Geology 233, 358–363.

Hacker, B.R., Ratschbacher, L., Webb, L., Ireland, T., Walker, D., Shuwen, D., 1998. U/Pb zircon ages constrain the architecture of the ultrahigh-pressure Qinling-Dabie Orogen, China. Earth and Planetary Science Letters 161, 215–230.

Halpin, J.A., Gerakiteys, C.L., Clarke, G.L., Belousova, E.A., Griffin, W.L., 2005. In-situ U–Pb geochronology and Hf isotope analyses of the Rayner Complex, east Antarctica. Contributions to Mineralogy and Petrology 148, 689–706.

Hawkesworth, C.J., Dhuime, B., Pietranik, A.B., Cawood, P.A., Kemp, A.I.S., Storey, C.D., 2010. The generation and evolution of the continental crust. Journal of the Geological Society 167, 229–248.

Hoskin, P.W.O., Schaltegger, U., 2003. The composition of zircon and igneous and metamorphic petrogenesis. In: Hanchar, J.M., Hoskin, P.W.O. (Eds.), Zircon. Mineralogical Society of America, Washington, pp. 27–62.

Hu, Z., Liu, Y., Gao, S., Liu, W., Zhang, W., Tong, X., Lin, L., Zong, K., Li, M., Chen, H., Zhou, L., Yang, L., 2012. Improved in situ Hf isotope ratio analysis of zircon using newly designed X skimmer cone and jet sample cone in combination with the addition of nitrogen by laser ablation multiple collector ICP-MS. Journal of Analytical Atomic Spectrometry 27, 1391–1399.

Huang, J., Zheng, Y., Zhao, Z., Wu, Y., Zhou, J., Liu, X., 2006. Melting of subducted continent: element and isotopic evidence for a genetic relationship between

Neoproterozoic and Mesozoic granitoids in the Sulu orogen. Chemical Geology 229, 227–256.

Jackson, S.E., Pearson, N.J., Griffin, W.L., Belousova, E.A., 2004. The application of laser ablation-inductively coupled plasma-mass spectrometry to in situ U–Pb zircon geochronology. Chemical Geology 211, 47–69.

Jahn, B.M., Auvray, B., Cornichet, J., Bai, Y.L., Shen, Q.H., Liu, D.Y., 1987. 3.5 Ga old amphibolites from eastern Hebei Province, China: field occurrence, petrography, Sm–Nd isochron age and REE geochemistry. Precambrian Research 34, 311–346.

Jahn, B.M., Glikson, A.Y., Peucat, J.-J., Hickman, A.H., 1981. REE geochemistry and isotopic data of Archaean silicic volcanics and granitoids from the Pilbara Block, western Australia: implications for the early crustal evolution. Geochimica et Cosmochimica Acta 45, 1633–1652.

Jiao, W.F., Wu, Y.B., Yang, S.H., Peng, M., Wang, J., 2009. The oldest basement rock in the Yangtze Craton revealed by zircon U–Pb age and Hf isotope composition. Science in China Series D: Earth Sciences 52, 1393–1399.

Kemp, A.I.S., Foster, G.L., Scherstén, A., Whitehouse, M.J., Darling, J., Storey, C., 2009. Concurrent Pb–Hf isotope analysis of zircon by laser ablation multi-collector ICP-MS, with implications for the crustal evolution of Greenland and the Himalayas. Chemical Geology 261, 244–260.

Kemp, A.I.S., Wilde, S.A., Hawkesworth, C.J., Coath, C.D., Nemchin, A., Pidgeon, R.T., Vervoort, J.D., DuFrane, S.A., 2010. Hadean crustal evolution revisited: new constraints from Pb–Hf isotope systematics of the Jack Hills zircons. Earth and Planetary Science Letters 296, 45–56.

King, P.L., Chappell, B.W., Allen, C.M., White, A.J.R., 2001. Are A-type granites the high-temperature felsic granites? Evidence from fractionated granites of the Wangrah Suite. Australian Journal of Earth Sciences 48, 501–514.

Kinny, P.D., Compston, W., Williams, I.S., 1991. A reconnaissance ion-probe study of hafnium isotopes in zircons. Geochimica et Cosmochimica Acta 55, 849–859.

Kinny, P.D., Maas, R., 2003. Lu–Hf and Sm–Nd isotope systems in zircon. In: Hanchar, J.M., Hoskin, P.W.O. (Eds.), Zircon. The Geological Society of America, Washington, USA, pp. 327–341.

Kusky, T.M., Windley, B.F., Zhai, M.G., 2007. Tectonic evolution of the North China Block: from orogen to craton to orogen, vol. 280. Geological Society, London, pp. 1–34 (Special Publications).

Li, S., Zhao, G., Santosh, M., Liu, X., Dai, L., Suo, Y., Tam, P.Y., Song, M., Wang, P., 2012. Paleoproterozoic structural evolution of the southern segment of the Jiao-Liao-Ji Belt, North China Craton. Precambrian Research 200-203, 59–73.

Li, X.P., Zheng, Y.F., Wu, Y.B., Chen, F.K., Gong, B., Li, Y.L., 2004. Low-T eclogite in the Dabie terrane of China: petrological and isotopic constraints on fluid activity and radiometric dating. Contributions to Mineralogy and Petrology 148, 443–470.

Li, Z., Li, X., Zhou, H., Kinny, P.D., 2002. Grenvillian continental collision in south China: new SHRIMP U–Pb zircon results and implications for the configuration of Rodinia. Geology 30, 163–166.

Ling, W.L., Gao, S., Zheng, H.F., Zhou, L., Zhao, Z.B., 1998. An Sm–Nd isotopic dating study of the Archean Kongling complex in the Huangling area of the Yangtze craton. Chinese Science Bulletin 43, 1187–1191.

Liu, C., Zhao, G., Sun, M., Zhang, J., Yin, C., He, Y., 2012a. Detrital zircon U–Pb dating, Hf isotopes and whole-rock geochemistry from the Songshan Group in the Dengfeng Complex: constraints on the tectonic evolution of the Trans-North China Orogen. Precambrian Research 192–195, 1–15.

Liu, D.Y., Nutman, A.P., Compston, W., Wu, J.S., Shen, Q.H., 1992. Remnants of ≥3800 Ma crust in the Chinese part of the Sino-Korean craton. Geology 20, 339–342.

Liu, F., Guo, J., Peng, P., Qian, Q., 2012b. Zircon U–Pb ages and geochemistry of the Huai'an TTG gneisses terrane: petrogenesis and implications for ~2. 5 Ga crustal growth in the North China Craton. Precambrian Research 212–213, 225–244.

Liu, X.M., Gao, S., Diwu, C.R., Ling, W.L., 2008a. Precambrian crustal growth of Yangtze craton as revealed by detrital zircon studies. American Journal of science 308, 421–468.

Liu, Y.S., Zong, K.Q., Kelemen, P.B., Gao, S., 2008b. Geochemistry and magmatic history of eclogues and ultramafic rocks from the Chinese continental scientific drill hole: subduction and ultrahigh-pressure metamorphism of lower crustal cumulates. Chemical Geology 247, 133–153.

Liu, Y.S., Hu, Z.C., Gao, S., Gunther, D., Xu, J., Gao, C.G., Chen, H.H., 2008c. In situ analysis of major and trace elements of anhydrous minerals by LA-ICP-MS without applying an internal standard. Chemical Geology 257, 34–43.

Liu, Y.S., Gao, S., Hu, Z.C., Gao, C.G., Zong, K.Q., Wang, D.B., 2010a. Continental and oceanic crust recycling-induced melt-peridotite interactions in the Trans-North China Orogen: U–Pb dating, Hf isotopes and trace elements in zircons from mantle xenoliths. Journal of Petrology 51, 537–571.

Liu, Y.S., Hu, Z.C., Zong, K.Q., Gao, C.G., Gao, S., Xu, J.A., Chen, H.H., 2010b. Reappraisal and refinement of zircon U–Pb isotope and trace element analyses by LA-ICP-MS. Chinese Science Bulletin 55, 1535–1546.

Loiselle, M.C., Wones, D.R., 1979. Characteristics and origin of anorogenic granites. Geological Society of America Abstracts with Programs 11, 468.

Lü, B., Zhai, M., Li, T., Peng, P., 2012. Zircon U–Pb ages and geochemistry of the Qinglong volcano-sedimentary rock series in Eastern Hebei: Implication for ~2500 Ma intra-continental rifting in the North China Craton. Precambrian Research 208–211, 145–160.

Martin, H., 1987. Petrogenesis of Archean trondhjemites, tonalites, and granodiorites from Eastern Finland-major and trace-element geochemistry. Journal of Petrology 28, 921–953.

Martin, H., 1994. The Archean grey gneisses and the genesis of continental crust. In: Condie, K.C. (Ed.), Developments in Precambrian Geology. Elsevier, pp. 205–259 (Chapter 6).

Martin, H., Smithies, R.H., Rapp, R., Moyen, J.F., Champion, D., 2005. An overview of adakite, tonalite–trondhjemite–granodiorite (TTG), and sanukitoid: relationships and some implications for crustal evolution. Lithos 79, 1–24.

McDonough, W.F., Sun, S.S., 1995. The composition of the Earth. Chemical Geology 120, 223–253.

Moyen, J.-F., Martin, H., 2012. Forty years of TTG research. Lithos 148, 312–336.

Nutman, A.P., Wan, Y., Du, L., Friend, C.R.L., Dong, C., Xie, H., Wang, W., Sun, H., Liu, D., 2011. Multistage late Neoarchaean crustal evolution of the North China Craton, eastern Hebei. Precambrian Research 189, 43–65.

O'Connor, J.T., 1965. A classirication for quartz-rich igneous rocks based on feldspar ratios. Geological Survey Professional Paper, 525-B, pp. 79–84.

Patchett, P.J., 1983. Importance of the Lu–Hf isotopicsystem in studies of planetary chronology and chemical evolution. Geochimica et Cosmochimica Acta 47, 81–91.

Pearce, J.A., Harris, N.B.W., Tindle, A.G., 1984. Trace element discrimination diagrams for the tectonic interpretation of granitic rocks. Journal of Petrology 25, 956–983.

Peng, M., Wu, Y.B., Gao, S., Zhang, H.F., Wang, J., Liu, X.C., Gong, H.J., Zhou, L., Hu, Z.C., Liu, Y.S., Yuan, H.L., 2012a. Geochemistry, zircon U–Pb age and Hf isotope compositions of Paleoproterozoic aluminous A-type granites from the Kongling terrain, Yangtze Block: constraints on petrogenesis and geologic implications. Gondwana Research 22, 140–151.

Peng, P., Guo, J.H., Windley, B.F., Li, X.H., 2011. Halaqin volcano-sedimentary succession in the central-northern margin of the North China Craton: products of Late Paleoproterozoic ridge subduction. Precambrian Research 187, 165–180.

Peng, T., Fan, W., Peng, B., 2012b. Geochronology and geochemistry of late Archean adakitic plutons from the Taishan granite-greenstone Terrain: implications for tectonic evolution of the eastern North China Craton. Precambrian Research 208–211, 53–71.

Qiu, Y.M., Gao, S., McNaughton, N.J., Groves, D.I., Ling, W., 2000. First evidence of >3.2 Ga continental crust in the Yangtze craton of south China and its implications for Archean crustal evolution and Phanerozoic tectonics. Geology 28, 11–14.

Rino, S., Komiya, T., Windley, B.F., Katayama, I., Motoki, A., Hirata, T., 2004. Major episodic increases of continental crustal growth determined from zircon ages of river sands; implications for mantle overturns in the Early Precambrian. Physics of the Earth and Planetary Interiors 146, 369–394.

Rowley, D.B., Xue, F., Tucker, R.D., Peng, Z.X., Baker, J., Davis, A., 1997. Ages of ultrahigh pressure metamorphism and protolith orthogneisses from the eastern Dabie Shan: U/Pb zircon geochronology. Earth and Planetary Science Letters 151, 191–203.

Rubatto, D., 2002. Zircon trace element geochemistry: partitioning with garnet and the link between U–Pb ages and metamorphism. Chemical Geology 184, 123–138.

Rudnick, R.L., Shan, G., Ling, W.L., Liu, Y.S., McDonough, W.F., 2004. Petrology and geochemistry of spinel peridotite xenoliths from Hannuoba and Qixia, North China craton. Lithos 77, 609–637.

Scherer, E., Munker, C., Mezger, K., 2001. Calibration of the lutetium–hafnium clock. Science 293, 683–687.

Smithies, R.H., Champion, D.C., Cassidy, K.F., 2003. Formation of earth's early Archaean continental crust. Precambrian Research 127, 89–101.

Soderlund, U., Patchett, J.P., Vervoort, J.D., Isachsen, C.E., 2004. The 176Lu decay constant determined by Lu–Hf and U–Pb isotope systematics of Precambrian mafic intrusions. Earth and Planetary Science Letters 219, 311–324.

Song, B.A., Nutman, A.P., Liu, D.Y., Wu, J.S., 1996. 3800 to 2500 Ma crustal evolution in the Anshan area of Liaoning Province, northeastern China. Precambrian Research 78, 79–94.

Sun, M., Chen, N., Zhao, G., Wilde, S.A., Ye, K., Guo, J., Chen, Y., Yuan, C., 2008. U–Pb zircon and Sm–Nd isotopic study of the Huangtuling granulite, Dabie-Sulu belt, China: implication for the paleoproterozoic tectonic history of the Yangtze Craton. American Journal of Science 308, 469–483.

Taylor, S.R., McLennan, S.M., 1985. The Continental Crust: Its Composition and Evolution. Blackwell Scientific, Oxford.

Vervoort, J.D., Patchett, P.J., 1996. Behavior of hafnium and neodymium isotopes in the crust: constraints from Precambrian crustally derived granites. Geochimica et Cosmochimica Acta 60, 3717–3733.

Vervoort, J.D., Patchett, P.J., Gehrels, G.E., Nutman, A.P., 1996. Constraints on early Earth differentiation from hafnium and neodymium isotopes. Nature 379, 624–627.

Vervoort, J.D., Blichert-Toft, J., 1999. Evolution of the depleted mantle: Hf isotope evidence from juvenile rocks through time. Geochimica et Cosmochimica Acta 63, 533–556.

Whalen, J.B., Currie, K.L., Chappell, B.W., 1987. A-type granites: geochemical characteristics, discrimination and petrogenesis. Contributions to Mineralogy and Petrology 95, 407–419.

Woodhead, J., Hergt, J., Shelley, M., Eggins, S., Kemp, R., 2004. Zircon Hf-isotope analysis with an excimer laser, depth profiling, ablation of complex geometries, and concomitant age estimation. Chemical Geology 209, 121–135.

Wu, F., Yang, Y., Xie, L., Yang, J., Xu, P., 2006. Hf isotopic compositions of the standard zircons and baddeleyites used in U–Pb geochronology. Chemical Geology 234, 105–126.

Wu, F., Zhang, Y.B., Yang, J.H., Xie, L.W., Yang, Y.H., 2008a. Zircon U–Pb and Hf isotopic constraints on the Early Archean crustal evolution in Anshan of the North China Craton. Precambrian Research 167, 339–362.

Wu, Y., Gao, S., Gong, H.J., Xiang, H., Jiao, W.F., Yang, S.H., Liu, Y.S., Yuan, H.L., 2009. Zircon U–Pb age, trace element and Hf isotope composition of Kongling

terrane in the Yangtze Craton: refining the timing of Palaeoproterozoic high-grade metamorphism. Journal of Metamorphic Geology 27, 461–477.

Wu, Y., Gao, S., Zhang, H., Zheng, J., Liu, X., Wang, H., Gong, H., Zhou, L., Yuan, H., 2012. Geochemistry and zircon U–Pb geochronology of Paleoproterozoic arc related granitoid in the Northwestern Yangtze Block and its geological implications. Precambrian Research 200–203, 26–37.

Wu, Y.B., Zheng, Y.F., Gao, S., Jiao, W.F., Liu, Y.S., 2008b. Zircon U–Pb age and trace element evidence for Paleoproterozoic granulite-facies metamorphism and Archean crustal rocks in the Dabie Orogen. Lithos 101, 308–322.

Xiong, Q., Zheng, J., Yu, C., Su, Y., Tang, H., Zhang, Z., 2009. Zircon U–Pb age and Hf isotope of Quanyishang A-type granite in Yichang: signification for the Yangtze continental cratonization in Paleoproterozoic. Chinese Science Bulletin 54, 436–446.

Yang, J.S., Wooden, J.L., Wu, C.L., Liu, F.L., Xu, Z.Q., Shi, R.D., Katayama, I., Liou, J.G., Maruyama, S., 2003. SHRIMP U–Pb dating of coesite-bearing zircon from the ultrahigh-pressure metamorphic rocks, Sulu terrane, east China. Journal of Metamorphic Geology 21, 551–560.

Zeh, A., Gerdes, A., Klemd, R., Barton, J.M., 2007. Archaean to Proterozoic Crustal evolution in the Central Zone of the Limpopo Belt (South Africa-Botswana): constraints from combined U–Pb and Lu–Hf isotope analyses of zircon. Journal of Petrology 48, 1605–1639.

Zeh, A., Gerdes, A., Barton, J.M., 2009. Archean accretion and crustal evolution of the Kalahari Craton-the zircon age and Hf isotope record of granitic rocks from Barberton/Swaziland to the Francistown Arc. Journal of Petrology 50, 933–966.

Zeh, A., Gerdes, A., Barton, J., Klemd, R., 2010. U–Th–Pb and Lu–Hf systematics of zircon from TTG's, leucosomes, meta-anorthosites and quartzites of the Limpopo Belt (South Africa): constraints for the formation, recycling and metamorphism of Palaeoarchaean crust. Precambrian Research 179, 50–68.

Zeh, A., Gerdes, A., Millonig, L., 2011. Hafnium isotope record of the Ancient Gneiss Complex, Swaziland, southern Africa: evidence for Archaean crust–mantle formation and crust reworking between 3.66 and 2.73 Ga. Journal of the Geological Society 168, 953–963.

Zhai, M., Li, T., Peng, P., Hu, B., Liu, F., Zhang, Y., 2010. Precambrian Key Tectonic Events and Evolution of the North China Craton, vol. 338. Geological Society, London, pp. 235–262 (Special Publications).

Zhai, M., Santosh, M., 2011. The early Precambrian odyssey of the North China Craton: a synoptic overview. Gondwana Research 20, 6–25.

Zhang, S.B., Zheng, Y.F., Wu, Y.B., Zhao, Z.F., Gao, S., Wu, F.Y., 2006a. Zircon isotope evidence for ≥3.5 Ga continental crust in the Yangtze craton of China. Precambrian Research 146, 16–34.

Zhang, S.B., Zheng, Y.F., Wu, Y.B., Zhao, Z.F., Gao, S., Wu, F.Y., 2006b. Zircon U–Pb age and Hf isotope evidence for 3.8 Ga crustal remnant and episodic reworking of Archean crust in South China. Earth and Planetary Science Letters 252, 56–71.

Zhang, S.B., Zheng, Y.F., Wu, Y.B., Zhao, Z.F., Gao, S., Wu, F.Y., 2006c. Zircon U–Pb age and Hf–O isotope evidence for Paleoproterozoic metamorphic event in South China. Precambrian Research 151, 265–288.

Zhang, S.B., Zheng, Y.F., Zhao, Z.F., Wu, Y.B., Yuan, H.L., Wu, F.Y., 2008. Neoproterozoic anatexis of Archean lithosphere: geochemical evidence from felsic to mafic intrusions at Xiaofeng in the Yangtze Gorge, South China. Precambrian Research 163, 210–238.

Zhang, S.B., Zheng, Y.F., Zhao, Z.F., Wu, Y.B., Yuan, H.L., Wu, F.Y., 2009. Origin of TTG-like rocks from anatexis of ancient lower crust: geochemical evidence from Neoproterozoic granitoids in South China. Lithos 113, 347–368.

Zhao, G.C., Wilde, S.A., Cawood, P.A., Sun, M., 2001. Archean blocks and their boundaries in the North China Craton: lithological, geochemical, structural and P-T path constraints and tectonic evolution. Precambrian Research 107, 45–73.

Zhao, G.C., Sun, M., Wilde, S.A., Li, S.Z., 2005. Late Archean to Paleoproterozoic evolution of the North China Craton: key issues revisited. Precambrian Research 136, 177–202.

Zheng, J., Griffin, W.L., O'Reilly, S.Y., Lu, F., Wang, C., Zhang, M., Wang, F., Li, H., 2004. 3.6 Ga lower crust in central China: new evidence on the assembly of the North China craton. Geology 32, 229–232.

Zheng, J.P., Griffin, W.L., O'Reilly, S.Y., Zhang, M., Pearson, N., Pan, Y.M., 2006. Widespread Archean basement beneath the Yangtze craton. Geology 34, 417–420.